DESIGN OF PASSIVE RADIATIVE SURFACES FOR ENERGY-EFFICIENT BASE STATION COOLING

by

AHMET CAN ŞUYUN

Submitted to Graduate School of Engineering and Natural Sciences

in partial fulfillment of

the requirement for the degree of Master of Science

Sabanci University

July 2023

DESIGN OF PASSIVE RADIATIVE SURFACES FOR ENERGY-EFFICIENT BASE STATION COOLING

Approved by:

Assist. Prof. Korkut Kaan Tokgöz…….

(Thesis Supervisor)

Prof. Dr. Serhat Yeşilyurt……..

(Thesis Co-Supervisor)

Prof. Dr. Gözde İnce…….

Prof. Dr. İbrahim Tekin…….

Assoc. Prof. Onur Taylan……..

Date of Approval: July 25, 2023

ABSTRACT

DESIGN OF PASSIVE RADIATIVE SURFACES FOR ENERGY-EFFICIENT BASE STATION COOLING

AHMET CAN ŞUYUN

MECHATRONICS ENGINEERING, M.SC. THESIS, JULY 2023

Thesis Supervisor: Assist. Prof. Korkut Kaan Tokgöz

Thesis Co-Supervisor: Prof. Dr. Serhat Yeşilyurt

Keywords: natural convection, optical thin-films, passive radiative cooling, thermal radiation, 5g small cell base station

It is estimated that 65 million 5G base stations are needed worldwide due to the increasing number of internet users and IoT applications. Switching to 5G would require a denser base station network due to the higher path loss at higher frequencies to supply the required higher data rate demand per user. This would increase energy consumption for connectivity as a whole. For a vast number of base stations, it would require enormous amounts of energy to keep them at suitable operation temperature in addition to their intrinsic signal processing and propagation-related power consumption. The aim of this thesis is to investigate, design and analyze possible solutions to decrease energy consumption for cooling base stations. Natural convection cooling and passive radiative cooling are the two passive cooling solutions, which do not require any additional energy consumption, and are investigated in this thesis. It is discovered that under solar radiation for a moderate summer day, natural

convection, practically applied for many base stations, is not enough to cool a small cell base station. To be able to decrease the effect of heat from solar radiation, two novel optical surfaces are designed to reflect solar radiation and radiate thermal energy to outer space. Since these surfaces are used in a wireless communication device, one of the surfaces is designed to transmit microwaves and millimeter waves, meanwhile reflecting solar radiation, and emitting thermal radiation in the atmospheric transmission window (ATW). With the titanium dioxide nanoparticles embedded in polymethyl methacrylate, 98% reflection in the solar band, and 4% reflection in ATW, along with over 98% transmission in microwave and millimeter wave frequencies, were achieved. The second optical surface is designed as multi-layer thin film. With four layers of thin films and an aluminum sub-layer, 91% reflection in solar band, and 20% reflection in ATW were achieved. As a result of these studies, electronic equipment that operates with 5W can be cooled without any electric consumption.

ÖZET

BAZ İSTASYONLARININ ENERJİ TASARRUFLU SOĞUTMASI İÇİN PASİF IŞINIMLI YÜZEY TASARIMI

AHMET CAN ŞUYUN

MEKATRONİK MÜHENDİSLİĞİ YÜKSEK LİSANS TEZİ, TEMMUZ 2023

Tez Danışmanı: Assist. Prof. Korkut Kaan Tokgöz

Tez Eş Danışmanı: Prof. Dr. Serhat Yeşilyurt

Anahtar Kelimeler: doğal konveksiyon, optik ince film, pasif ışınımsal soğutma, ışınımla ısı transferi, 5G baz istasyonu

Artan internet kullanıcı sayısı ve IoT uygulamaları nedeniyle dünya genelinde 65 milyon adet 5G baz istasyonuna ihtiyaç duyulduğu öngörülmektedir. 5G'ye geçiş, yüksek frekansta daha yüksek yol kaybı nedeniyle gereksinim duyulan daha yüksek veri hızı talebini karşılayabilmek için daha yoğun bir baz istasyonu ağı gerektirir. Bağlanabilirlik için gereken enerji miktarı bu nedenle artış gösterecektir. Sayısal işaret işlemleri ve yayınım için harcanan enerjinin yanında yüksek sayıdaki baz istasyonunu uygun kullanım sıcaklığında tutmak için kayda değer miktarda enerji harcamak gerekmektedir. Bu tezin amacı, baz istasyonlarını soğutmak için harcanan enerjinin nasıl azaltılacağı ile ilgili muhtemel çözümlerin tasarım ve analizini araştırmaktır. Enerji tüketmeyen iki soğutma metodu olan doğal konveksiyon ve pasif ışınımsal soğutma bu çalışma içerisinde incelenmiştir. Güneş ışığına doğrudan maruz kalan bir baz istasyonunun 5G baz istasyonunu soğutmak için doğal konveksiyonun yeterli

olmadığı görülmüştür. Güneşin etkisini azaltabilmek için, güneş ışınımını yansıtacak ve termal enerjiyi uzaya yayacak iki yeni optik yüzey tasarlanmıştır. Bu yüzeyler kablosuz iletişim cihazlarında kullanılacağı için, yüzeylerden biri mikrodalga ve milimetre dalgalarını iletebilecek, aynı zamanda güneş ışınımını yansıtıp, atmosferik iletim penceresinde termal ışıma yapabilecek şekilde tasarlanmıştır. Polimetil metakrilat içerisine gömülü titanium dioksit nanoparçaçıkları güneş ışınımı tayfında %98, atmosferik iletim penceresinde %4 yansıma elde ederken, mikrodalga ve milimetre dalga frekanslarında %98'in üzerinde geçirgenlik sağlanmıştır. İkinci optic yüzey çok katmanlı ince filmler olarak tasarlanmıştır. Dört katman ince film ve alüminyum alt tabake ile güneş ışınımı tayfında %91 yansıma ve atmosferik iletim penceresinde %20 yansıma elde edilmişir. Bu çalışmaların sonucunda 5W güç ile çalışan elektronik ekipmanların herhangi bir elektrik tüketimi olmaksızın soğutulabileceği sonucuna varılmıştır.

ACKNOWLEDGEMENTS

I would like to express my sincere gratitude to my advisor and co-advisor, Assist. Prof. Korkut Kaan Tokgöz and Prof. Dr. Serhat Yeşilyurt, for their invaluable guidance and support throughout my master's program. Their expertise and encouragement helped me to complete this research and write this thesis.

I would also like to thank Prof. Dr. Gözde İnce, Prof. Dr. İbrahim Tekin and Assoc. Prof. Onur Taylan for serving on my thesis committee and providing helpful feedback and suggestions.

I would also like to thank my friends and family for their love and support during this process. Without them, this journey would not have been possible.

To my dearest

Burcu

Table of Contents

List of Figures

List of Tables

1. INTRODUCTION

1.1. Background & Motivation

There are 1.4 million 5G base stations in China (Jiang, 2023). It is planned to triple the number by 2025. It is estimated that 65 million 5G base station is needed worldwide due to the increasing number of internet users and IoT application (Chang, 2020). Switching to 5G would require a denser base station network that operates at higher frequencies for higher data transfer rates. This would increase overall 5G network energy consumption for connectivity because higher frequencies tend to have higher path loss as can be seen in Figure 1.1-1 (Chih-Lin I, 2020).

Since each 5G small cell consumes 25 W to 40 W (Mingjie Feng, 2017), for a vast number of base stations it would require an enormous amount of energy to keep them at suitable operation temperature. Forced cooling is widely used in base stations (Rang Tu, 2010). 30-50% of the power input of base stations is consumed by cooling systems (Rang Tu, 2010). It can be estimated that for a base station that operates with 20 W of power, 8.5 W to 20 W power is needed to cool the base station. Semiconductor technologies continue to advance exponentially each year. Improvement in manufacturing capabilities makes production of smaller transistors possible which results in higher computational power per unit volume in processors (Incropera, 1969).

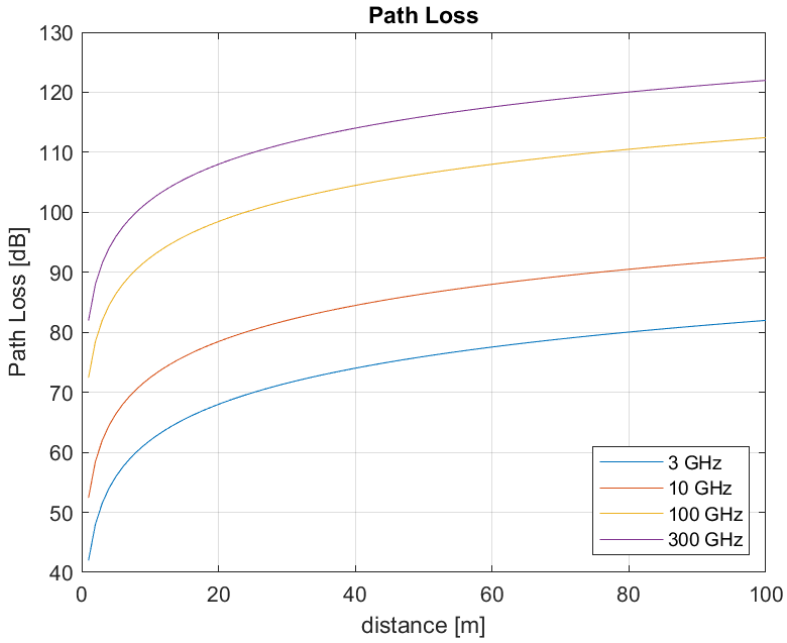

Figure 1-1 Path loss of different frequencies (Şuyun, 2023)

It becomes harder for engineers to design cooling systems since higher computational power per unit volume results in more heat generation in smaller volumes. Cooling techniques should also keep up with the increase in computational power since it is important to keep the temperature of electronic equipment low, to increase its lifetime (Black, 1969).

The median time to failure (MTF) of electronic equipment is dependent on the operation temperature as Black's equation shows (Black, 1969),

Equation 1 Black's Equation

$$\mathrm{MTF} = \frac{1}{\mathrm{AJ}^2} \exp\left(\frac{\mathrm{E_A}}{\mathrm{K_B T}}\right)$$

Where;

A: Constant

J: Current Density [$^{\mathrm{A}}/_{\mathrm{cm}^2}$]

$\mathrm{E_A}$: Active Energy [eV]

$\mathrm{K_B}$: Boltzmann Constant

T: Operation Temperature

The equation suggests that with the increase in the temperature, the median time to failure decreases which results in a shorter lifetime for the electronic component.

It is important to cool base stations, however, cooling the base stations with conventional cooling methods can create new problems. For forced convection air cooling, a driving fan is needed to guide air through the surface of the electronic equipment. The driving fan needs power input to operate meanwhile it can cause noise during operation (Sohel Murshed, 2017). Liquid cooling may provide higher performance than forced convection air cooling, however, it suffers from complexity and high-maintenance needs (Sohel Murshed, 2017). Leaks in liquid cooling systems are more likely to create catastrophic failures.

1.2. Aims and Objectives

The aim of this thesis is to investigate design and analyze possible passive cooling solutions to decrease energy demand for cooling base stations. Conventionally base stations are cooled either liquid or forced convection. With passive cooling solutions energy demand as well as maintenance and operational costs for cooling can be reduced. Temperature increase or decrease of a base station box depends on the radiative properties of the environment and ambient air temperature. Base stations can be located between buildings or in open fields, also they can be located on a pole placed on asphalt or sand, etc. The conceptual 5G Base Station is shown in Figure 1-3. At the top of the cell, a square hole with a mesh in the entry can be seen. This square hole continues through the cell. It can be assumed as a square shaft in the middle of the base station. Flow analysis and the effect of thermal radiation for this square shaft is worked with commercial computer programs and analytical solutions.

Figure 1-2 Small cell base station (creativecommons, 2023)

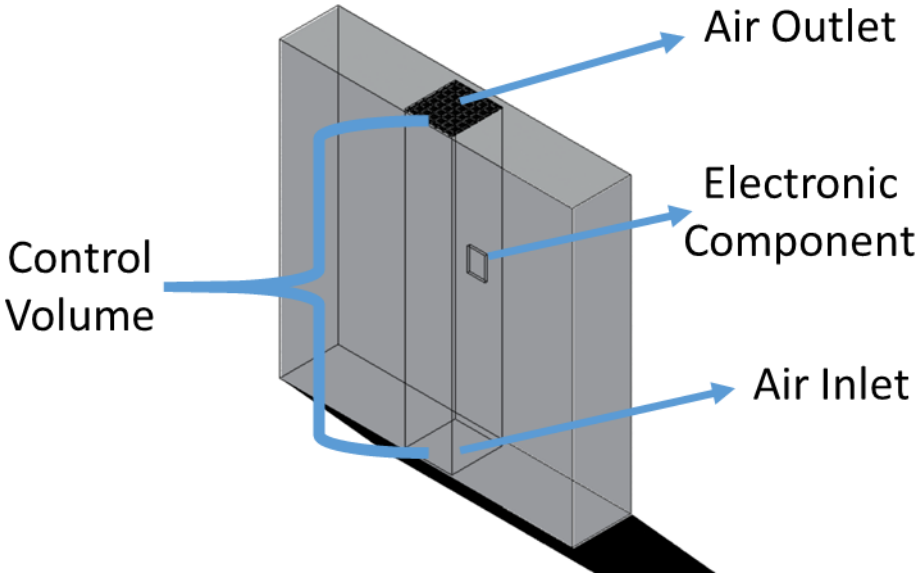

Figure 1-3 Render of Conceptual 5G Small Cell with Electronic Chip in the Middle (Şuyun, 2023)

Passive radiative cooling surfaces aim to radiate heat to outer space. In this thesis, passive radiative cooling surfaces and fins for natural convective cooling are used to decrease cooling power requirements. The main objective is to eradicate the need for any system that require energy to operate or decrease energy demand since there would be vast amounts of base stations in the future.

Passive radiative daytime cooling surfaces which reflect incident solar radiation and absorbs radiation in atmospheric transmission window can help to reduce energy demand. Another energy-free cooling method is natural convection is designed by optimizing heat sink design.

1.3. Literature Survey

1.3.1. Fin Design Optimization for Natural Convection

In the past, RF systems did not require extensive cooling. With the new generation radio employing phased arrays heating becomes a problem. Computer chips have more transistors per unit volume as the transistors get smaller in dimension (Schaller, 1997). Higher computational capacity results in more heat generation in smaller volumes. Thus, cooling performance becomes crucial (Incropera, 1969). Fins are generally designed for forced convective cooling, and activated or their speed is increased once the electronic parts' temperature is in operational upper-temperature limit. More than 50% of the failures in the electronics components are due to high operation temperature (ASIAC, 1989; Pedram, 2006). Cooling techniques can be categorized into four groups. These techniques are liquid evaporation, forced liquid cooling, forced air-cooling, radiation, and free convection. Performance scale of the mentioned techniques can be seen in Table 1.

Table 1 Cooling Techniques and Corresponding Heat Removal Range (Scott, 1976)

Cooling Technique	**Heat Flux Range [kW/m^2]**
Radiation and Natural Convection	0.15-1.55
Forced Air-Cooling	0.8-16
Forced Liquid Cooling	11-1000
Evaporation Liquid	15.5-1000+

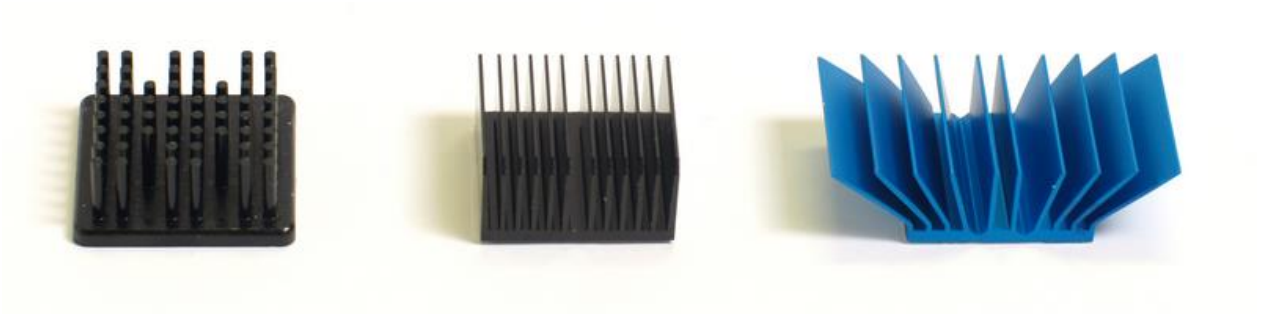

Figure 1-4 Pin, Straight and Flared Heat Sinks Respectively (Wikimedia, 2010)

Natural convection may suffer from a low heat removal rate as Table 1 suggests. However, it is cheaper to apply and does not have any moving parts, which results in higher reliability (Scott, 1976). It is the simplest cooling method in means of implementation. Cooling for power dissipation up to 5W can be possible with natural convection (Sohel Murshed, 2017).

Natural convection offers an energy-free solution. To increase the heat transfer area, the number of fins can be increased. However natural convection heat transfer rate does not necessarily increase as area increases. The orientation of heat sinks, the shape of each fin, or periodicity of fins are worked extensively to determine its effect on heat transfer by researchers and engineers (A. Bar-Cohen, 1984).

Multiple fins or columns are widely used in electronics cooling. Copper and aluminum are widely used due to their high thermal conductivity (Çengel, 2007; Remsburg, 2017). Heat sinks categorized according to their fin geometry are shown in Figure 1-4. Straight-fin heat sinks are cheaper to produce (Lee, 1995), since cost-effectiveness is concerned in this work, straight fin heat sink is examined.

1.3.2. Spectrally Selective Multilayer Thin Films for PRC Application

Thermal radiation occurs in any temperature above 0K. The universe itself can be considered as an infinite heat sink since its temperature is slightly above 0K. So, any object floating in the universe dissipates its heat into outer space with electromagnetic waves. When it comes to objects under our atmosphere, radiative heat transfer to outer space has constraints. Only some of the radiated thermal energy can be transferred to outer space. Our atmosphere has a

gap between that prevents radiation outside of the range 8 μm and 13 μm wavelength from dissipating to outer space. The wavelength gap which radiation can be radiated to outer space is called 'Atmospheric Transmission Window' (ATW). Earlier works on radiative cooling were nocturnal (Harrison AW, 1978; Michell D, 1979), which can create a cooling effect only during nighttime. Near black material on wide range of frequencies is used. These applications were ineffective in day light since they would absorb solar energy and cause overheating. The second type of radiative cooling has ability to continue cooling in daytime. If the surface of a body can reflect solar radiation and continue to radiate between ATW cooling effects can be observed. To achieve passive radiative cooling, it is not enough to tailor emissivity in 8 μm – 13 μm range unlike nocturnal passive radiative cooling, it is also important to reflect solar radiation (Zhao, 2019). Solar radiation is dominant in 500 nm, yet it is effective up to 3 μm wavelength. Recent works on passive radiative cooling surfaces rely on metasurfaces and photonic structures. Selective surfaces are designed and fabricated with modern techniques. Multilayer thin-film radiator is designed, fabricated, and tested by Raman (Raman AP, 2014). Radiator created a cooling effect that decreased temperature of the system 6 degrees below ambient temperature. There are several methods to obtain PRC surface. There are photonic radiators, nanoparticle-based radiators, film-based radiators and natural radiators that can create the passive radiative affect (Zhao, 2019).

Optical thin films are an area of interest in many disciplines. They are widely used in communication, solar power, and thermal management (Macleod, 2021). Thermal management can be done by making use of thermal radiation fundamentals which crosses paths with optical properties of materials. Each object above 0K emits energy by radiating. Objects at thermodynamic equilibrium emits and absorbs thermal electromagnetic radiation at every wavelength. It is possible to engineer reflection and absorption of a surface by adjusting thicknesses of multilayer thin films to create constructive and destructive optical interfaces for certain wavelength ranges (Willey, 2019). Using dielectric materials in multilayer films are widely used to reflect and absorb thermal radiation (Zhao, 2019). The thickness of each film is precisely calculated to create reflection or absorption effect on a specific band solely dependent on the application. Several examples are designed and analyzed with FDTD methods in thesis. Usual practice is stacking low refractive index and high refractive index materials on top of each other with specific thickness and number of

layers (Raman AP, 2014; Wu JY, 2017; Suichi T, 2017) . For solar reflecting surfaces common practice is using materials which are lossless under radiation with shorter wavelengths (0.3-3 um). Hafnium dioxide-silicon dioxide (Raman AP, 2014), Titanium dioxide-aluminum dioxide (Kecebas MA, 2017; Koucheh, 2021), calcium fluoride-germanium pairs (Huang Y, 2018) are used in previous works to achieve passive radiative cooling effect.

1.3.3. Spectrally Selective Titanium Dioxide Embedded Acrylic Coating for PRC Applications

Multi-layer dielectric thin-films are durable, but manufacturing cost of thin-films are higher than polymer coatings (Zhao, 2019). In means of ease of production, researchers proposed simpler methods using transparent polymer, acetone, water, and barium sulfate that can also create passive radiative cooling effect (Mandal, 2018). These materials can be found easily, and fabrication method does not require special laboratory equipment and process is not sensitive to environmental parameters unlike multilayer thin-film manufacturing methods including sputtering or atom layer deposition etc. (Piegari, 2018). Transparent polymer is dissolved in acetone, then water is added to solution. Then the solution is applied to the surface with a brush or a roller. When acetone and water are evaporated from the mixture, polymer with tiny pores is left behind. These pores are filled with air when acetone and water are evaporated. This new texture creates scattering effect due to the high number of high refractive index (transparent polymer) low refractive index (air) layers. In this case transparent polymer becomes a high index material meanwhile air in the pockets are low index material. High refractive index nanoparticles can also be embedded to transparent polymers to obtain same affect (Zhang, 2017). This time transparent polymer becomes low refractive index material.

1.4.Contributions

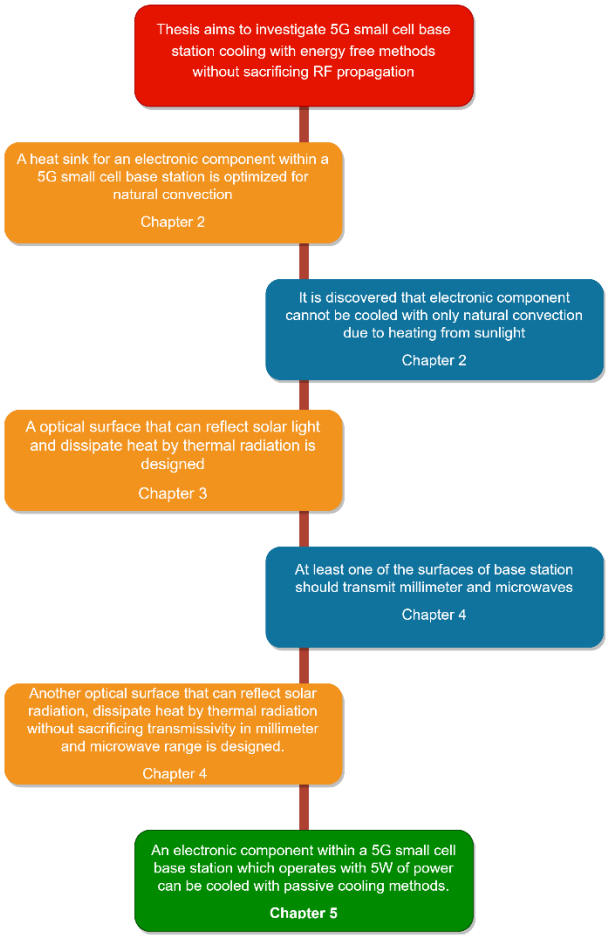

Figure 1-5 Flow Summary of Thesis (Şuyun, 2023)

The general flow of thesis is shown in Figure 1-6. Thesis aims to investigate energy free methods to keep 5G base station in suitable operation temperature. Cooling of base station by just natural convection is not sufficient under direct sunlight. Novel designs, which are investigated in this thesis, can prevent heating of base station due to solar irradiation. Additionally, these designs also can dissipate heat to outer space by thermal radiation. Meanwhile, at least one of the surfaces is designed to reflect sunlight, dissipate heat by thermal radiation and keep transmissivity in operating frequency of base station. At the end it is discovered that a small cell 5G base station can be operated under direct sunlight with the power input of 5W.

1.4.1. Fin Design Optimization for Natural Convection

The various number of fins, length of the fins, position of the microchip and length of the flow tube are studied in this thesis. Semi-empirical optimization techniques are used to increase performance of heat sink fins. Due to geometrical constraints and operational temperature of base station chip, final geometry of fins resulted in two fins. Heat sink with two fins does not need any metal cutting or extrusion process. By bending an aluminum plate final geometry can be easily achieved, thus decreasing cost for manufacturing.

1.4.2. Spectrally Selective Multilayer Thin Films for PRC Application

Dielectric materials can be stacked on top of each other layer by layer to create constructive/destructive interferences. Previous works used metals to reflect radiation in infrared region. In this thesis it is not possible to use reflective slab on bottom of titanium oxide and silicon oxide layers on all the surfaces, since it is aimed to transmit radiation in 8 μm – 13 μm wavelength range and radio waves in at least on side of the box. So, a methodology is developed to create multilayer of titanium oxide and silicon oxide thin-films, which reflect radiation in 0.3 μm – 3 μm wavelength range, while transmitting 8 μm – 13 μm wavelength range. Particle swarm optimization algorithm is used to optimize design parameters for such an objective. As layer number increases fabrication costs also increases. In this thesis, solutions for reflective coating with 2 layers are presented with analytical solution and FDTD analyses. For absorptive layer a single layer of silicon dioxide is used. With the aluminum base slab there are 4 layers in total which is an economical alternative in multilayer thin film design concept.

1.4.3. Spectrally Selective Titanium Dioxide Embedded Acrylic Coating for PRC Applications

Since all the sides of the base stations cannot be coated with PRC coatings with metal bottom layer, at least of the surfaces should be coated with a surface that transmits radio waves. Multilayer thin-films may give better reflection and absorption properties, however they suffer from expensive and precise manufacturing processes. For porous polymer solutions optical properties do not provide the same performance however they are cheaper to produce. Previous work on porous polymers relied on exotic plastics called $P(VdF\text{-}HFP)_{HP}$. In this thesis similar results are obtained with Polymethyl methacrylate **(**PMMA**)** which is a cheaper alternative to $P(VdF\text{-}HFP)_{HP.}$ In this thesis, PRC surface to be designed will be used in 5G base stations. Thus, design should be transparent to radio waves. Previous work on passive radiative cooling uses high reflective metal coating (Ag, Au, W etc.) to reflect longer wavelengths. Since metals highly reflect radio waves, they cannot be used in base stations. In other words, design should transmit electromagnetic waves in microwave and millimeter wave frequencies, while reflecting solar radiation between 0.3 μm – 3 μm wavelength and absorb/emit thermal energy between 8 μm – 13 μm wavelengths.

2. FIN DESIGN OPTIMIZATION FOR NATURAL CONVECTION

2.1. Problem Definition

Heat transfer occurs between any two points within a substance if there is a temperature difference in the substance. There are three types of heat transfer mechanisms. They are conduction, convection, and radiation. For heat transfer that occurs temperature difference and thermal resistance between two bodies are main determinants (KAMINSKI, 2017).

Equation 2 Heat Transfer Rate

$$\dot{Q} = hA_s(T_s - T_f)$$

Where,

$\dot{Q}: Heat\ transfer\ rate$

$h: Heat\ transfer\ coefficient$

$A_s: Surface\ area$

$T_s: Surface\ temperature$

$T_f: Fluid\ temperature$

Temperature profile may seem similar to forced convection however speed profile has different manner. As it gets further from the plate, flow speed decreases unlike forced

convection. Heat transfer coefficient of natural convection varies along the vertical position. Density variance due to temperature determines natural convection. Since velocity profile through the vertical surface is not constant, heat transfer coefficient changes with the vertical position. Heat transfer with natural convection is highly dependent on the density gradient in the volume of fluid. Fluid behavior is correlated with the change in density of fluid with respect to temperature. Figure 2-1 shows temperature and flow speed profile of fluid with respect to vertical plate. Buoyancy forces act on the fluid to create flow throughout the surface.

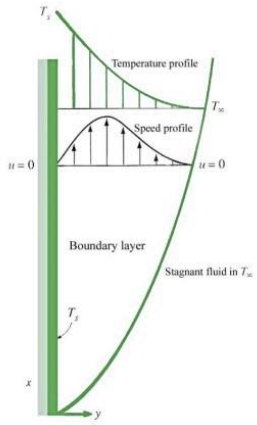

Figure 2-1 Natural Convection Flow and Temperature Characteristics *(Ozisik, 1985)*

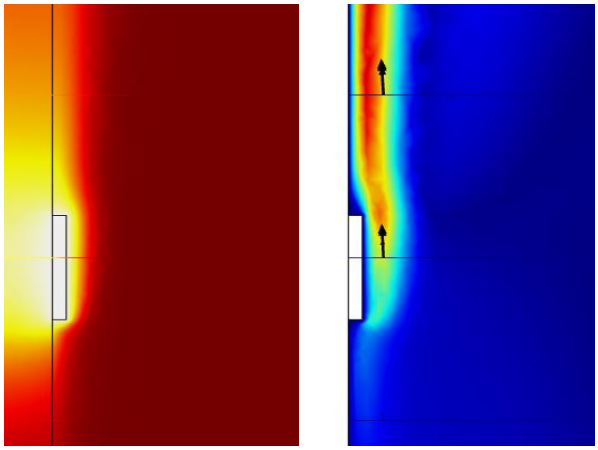

Figure 2-2 COMSOL Temperature and Flow Speed Analysis for Natural Convection on a Vertically Mounted Chip (Şuyun, 2023)

Volume expansivity β can be expressed as a function of fluid density ρ and temperature; Equation 3 Volume Expansivity

$$\beta = -\frac{1}{\rho}(\frac{\partial \rho}{\partial T})_p$$

Ideal gas law is written as following form to express temperature (T), pressure (P) dependency of density.

Equation 4 Ideal Gas Law

$$\rho = \frac{PM}{\bar{R}T^2}$$

While,

M:Molecular weight

$\bar{R}$:Universal gas constant

Surrounding pressure of the fluid assumed constant. Thus, with taking partial derivative of each side equation becomes;

Equation 5

$$(\frac{\partial \rho}{\partial T})_p = -\frac{PM}{\bar{R}T^2}$$

Then Volume expansivity β yields to

Equation 6

$$\beta = -\frac{1}{\rho}\left(\frac{\partial \rho}{\partial T}\right)_p = \frac{PM}{\rho \bar{R}T^2}$$

Since;

Equation 7

$$PM = \rho \bar{R}T$$

According to ideal gas law, volume expansivity $\beta = {}^{1}/_{T}$ for ideal gasses. To correlate natural convective flow Grashof number (Gr) is used;

Equation 8 Grashof Number

$$Gr = \frac{g\beta\rho^2(T_s - T_f)L_{char}^3}{\mu^2}$$

Since heat transfer coefficient is not constant through the surface average heat transfer coefficient is expressed as follows;

Equation 9 Nusselt Number

$$Nu = \frac{hL}{k} = CRa_L^n = C(Gr_lPr)^n$$

Meanwhile characteristic length L_{char} only depends on geometry, values C and n depend on both geometry and flow regime and thermal conductivity (k) depends on the material properties.

Where Rayleigh number Ra;

Equation 10 Rayleigh Number

$$Ra = \frac{g\beta\rho^2(T_s - T_f)L_{char}^3}{\mu^2}Pr$$

If there was not any extra measures to cool the chip, and assuming that chip does not stop working as its temperature increases flow regime inside the tube calculated by COMSOL can be seen in Figure 2-3.

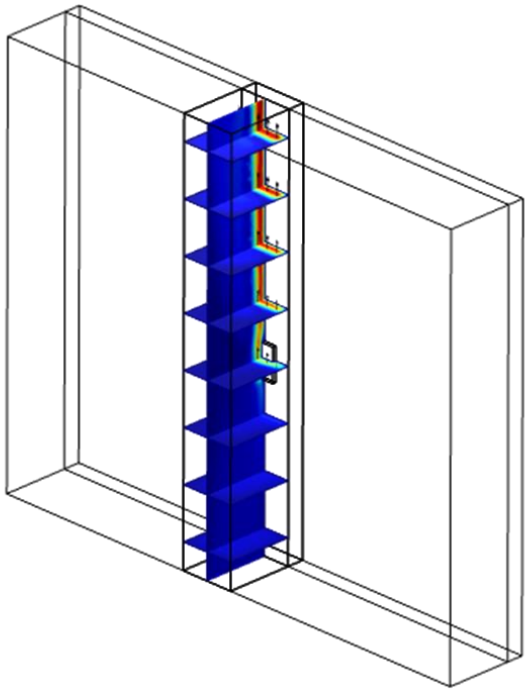

Figure 2-3 Natural Convection Flow Regime without any Cooling Measure (Şuyun, 2023)

The top and bottom surface of the rectangular prism is defined as an open boundary, meanwhile 435 W/m^2 inward heat flux is defined in front surface. There is not any forced convection, flow is non-isothermal flow where buoyancy is the only force driving fluid flow. Other faces of rectangular prism are considered as thermally insulated surfaces.

Average temperature of the chip with respect to applied power can be seen in Table 2

Table 2 Applied Power and Steady-State Chip Temperature

Applied Power	**Average Volume Temperature**
1 W	397K
5 W	685K
10 W	995K
20 W	1546K

2.2. Methodology

Assuming constant temperature 55-degree Celsius, optimized fins spacing can be found with the method explained by Bar-Cohen (A. Bar-Cohen, 1984);

For symmetric, isothermal plates total heat transfer rate Q_T can be found by;

Equation 11 Total Heat Transfer Rate in Isothermal Plates

$$Q_T = (2LS\Delta T)(m)(Nu\,{}^{k}/_{b})$$

Where,

m: $Number\ of\ plates$

L: $plate\ length$

S: $Plate\ width$

b: $Plate\ Spacing$

Optimum spacing b_{opt} can be found by

Equation 12 Optimum Spacing Between Straight Fins

$$b_{opt} = 2.714\frac{L_{char}}{Ra^{1/4}}$$

And heat transfer coefficient for optimum spacing is

Equation 13 Heat Transfer Coefficient

$$h = 1.31\frac{k}{S_{opt}}$$

For the parameters mentioned in the Table 3

Table 3 Parameters for Natural Convection

Parameter Description	**Value**
Width of the Base Plate	15 $[mm]$
Prandtl Number	0.709
Gravitational Acceleration	9.81 $\left[{}^{m}/_{s^2}\right]$
Surface Temperature	328 $[K]$
Ambient Temperature	303 $[K]$
Kinematic Viscosity	1.61 $[{}^{m^2}/_{s}]$

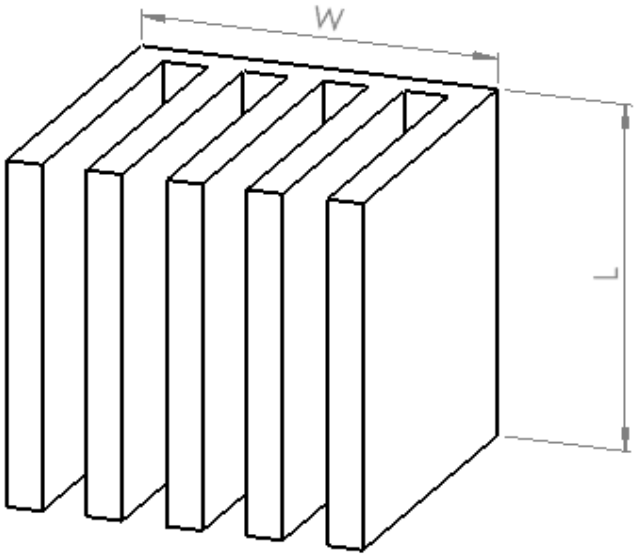

Figure 2-4 General Structure of Heat Sink (Şuyun, 2023)

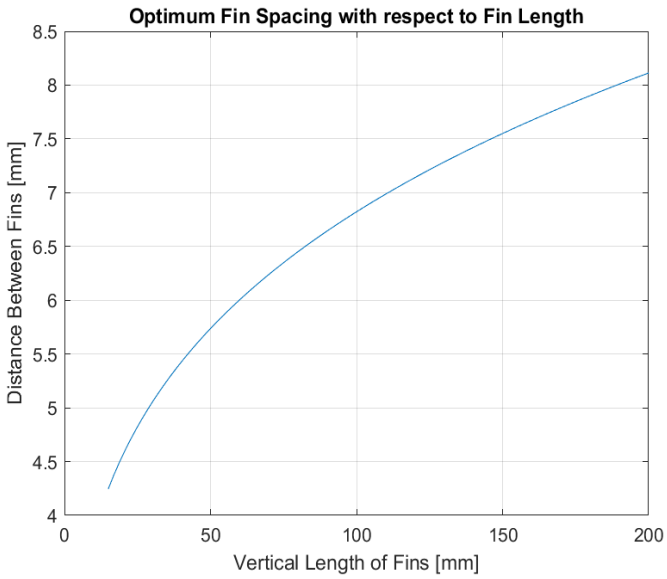

Figure 2-5 Optimum fin spacing with respect to Fin Length (L) (Şuyun, 2023)

As characteristic length L (Figure 2-2) of the fins increases optimum distance between fins also increases. Optimum fin spacing with respect to fin length can be seen in Figure 2.2-2. Flow in between plates of heat sinks can be assumed as isothermal vertical flat plates due to high thermal conductivity of aluminum fins. However, the walls of the shaft cannot be isothermal. Thus, optimum fins spacing found with mentioned method can only be starting point for optimization efforts.

Thermal radiation expressed as inward heat flux in simulations. 1000 W/m2 solar irradiation is considered (ASTM International, 2022). Solar flux can be calculated by making use of thermal radiation equations. Emissivity of the material, solar irradiation according to geographical location, atmospheric transmissivity and surface temperature of the object determines heat flux in/out of the object. Glass fiber reinforced polymer is widely used as a case material for base stations for its transmissivity in GHz band (Cary, 1974). However, GFRP composites suffer from high absorptivity in solar band. Emissivity of GFRP in solar and infrared band are (Adibekyan, 2019):

$$\varepsilon_{0.3\ \mu m-3\ \mu m} = 0.75$$

$$\varepsilon_{3\ \mu m-\infty} = 0.95$$

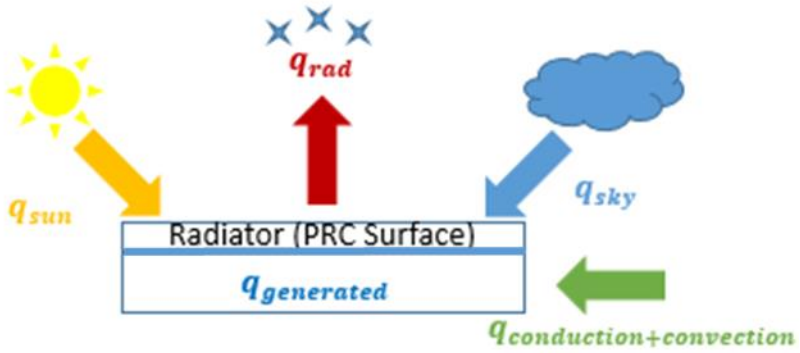

Figure 2-6 Thermal Equation Terms (Şuyun, 2023)

Thermal radiation heat flux per unit area can be found with thermal radiation equation with following methodology; General scheme has the characteristics above. Solar radiation, radiation from sky and ambient, heat generated within object, conduction and convection heat flux and radiated heat from object are the terms affecting the thermal equations. The temperature of object is assumed to be the same as the ambient temperature to simplify equations. Heat generated by the object and heat transfer due to convection calculated by computational fluid dynamics commercial program COMSOL Multiphysics®. So, three terms are calculated for the thermal radiation equations and superposed in COMSOL. Conduction heat transfer is also assumed as negligible since air surrounds the box and only connected with small connection elements.

With the assumptions above heating power due to thermal radiation becomes (Howell, 2021);

Equation 14 Thermal Radiation Equation

$$P_{total}(T_{object}) = P_{rad}(T_{object}) - P_{sun}(T_{sun})$$

Where;

T_{object}:Balance temperature of the object (303 [K])

T_{sun}:Blackbody temperature of the sun (5800 [K])

P_{total}:Total heat flux due to radiation

P_{rad}:Radiated heat flux by object

P_{sun}:Absorbed power due to solar radiation

Equation 15 Radiated Heat Flux from an Object

$$P_{rad}(T_{object}) = A \int d\Omega \cos\theta \int_0^{\infty} d\lambda I_{BB}(T_{object}, \lambda)\epsilon(\lambda, \theta)$$

Since object temperature is assumed as 303K and thermal radiation of object happens in longer wavelengths $P_{rad}(T_{object})$ can be simplified as;

$$P_{rad}(T_{object}) = \delta * A * T * \varepsilon_{3\ \mu m - \infty\ \mu m} * ({T_{object}}^4 - {T_{sky}}^4)$$

Where,

A:Area of the object (assumed as 1 m^2)

$\int d\Omega$:Angular integral over a sphere

λ:wavelength

$I_{BB}(T_{object},\lambda)$:Spectral radiance of a blackbody at temperature T_{object} can be found with (Howell, 2021)

Equation 16 Spectral Radiance of an Object

$$I_{BB}(T_{object}, \lambda) = \frac{2hc^2}{\lambda^5} \frac{1}{e^{hc/(\lambda k_B T_{object})} - 1}$$

Where;

h:Planck's constant

δ:Stefan-Boltzman Constant

k_B:Boltzmann constant

c:Speed of light

λ:wavelength

Absorbed power due to incident solar radiation can be calculated as:

Equation 17 Absorbed Solar Radiation

$$P_{sun} = A\int_0^{\infty} d\lambda \epsilon(\lambda, \theta_{sun}) I_{AM1.5}(\lambda)$$

Where,

$I_{AM1.5}(\lambda)$: Spectral Solar Irradiance $\left(1000 \frac{W}{m^2}\right)$ (ASTM International, 2022)

Flat plate with 1 m^2 with a fixed angle with respect to sun is assumed, so angular dependency on absorbed solar power is neglected. As it can be seen in Figure 2-5, peak wavelength for solar radiation is between 480 nm and 500 nm. For the objects around 300K, peak wavelength is around 10 µm. Emissivity of material is not same throughout the solar spectrum, so what fraction of the incident solar power is absorbed should be worked in detail (Howell, 2021). $F_{0\rightarrow\lambda T}$ is the fraction of radiation up to specified cut-off wavelength.

Equation 18 Fraction of Total Blackbody Intensity in Spectral Region 0 to $\lambda_{cut\text{-}off}$

$$F_{0\rightarrow\lambda_{cut-off}T} = \frac{15}{\pi^4}\sum_{m=1}^{\infty}\left[\frac{e^{-m\zeta}}{m}\left(\zeta^3 + \frac{3\zeta^2}{m} + \frac{6\zeta}{m^2} + \frac{6}{m^3}\right)\right]$$

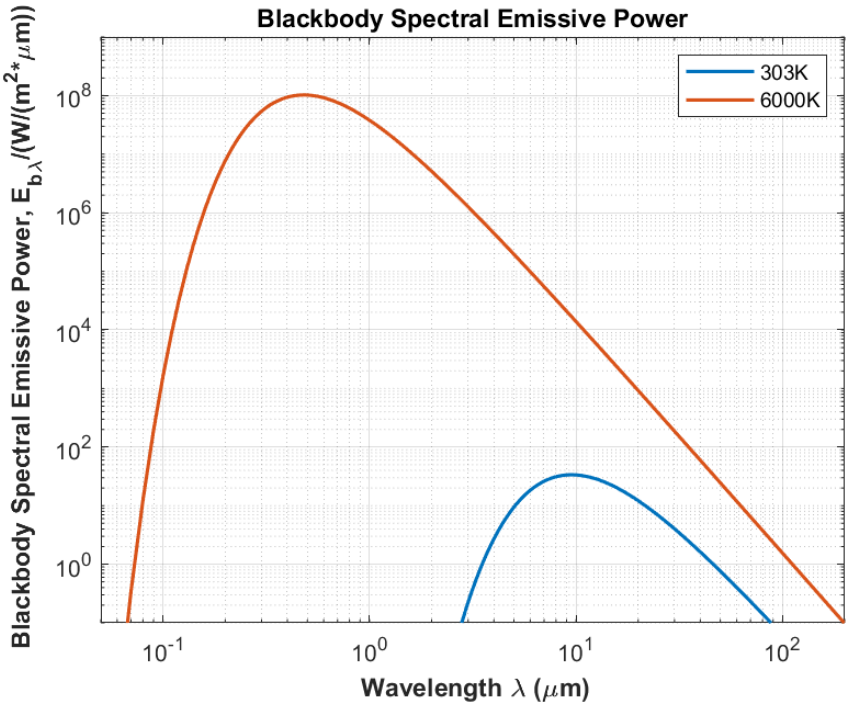

Figure 2-7 Blackbody Spectral Emissive Power with respect to Wavelength (Şuyun, 2023)

Where the quantity ζ is,

Equation 19

$$\zeta = {C_2}/{\lambda_{cut-off} T}$$

While,

Equation 20

$$C_2 = {h * c}/{\mathrm{k_B}}$$

Absorbed solar power:

$$P_{sun}(T_{sun}) = AF_{0\to\lambda_{cut-off}T} I_{AM1.5}(\lambda)\varepsilon_{0.3\ \mu m-3\ \mu m} + AF_{\lambda_{cut-off}T\to\infty} I_{AM1.5}(\lambda)\varepsilon_{3\ \mu m-\infty}$$

Cut-off wavelength $\lambda_{cut-off}$ is assumed as 3 µm, then $F_{0\to\lambda_{cut-off}T}$ becomes 98%. 98% of solar radiation has smaller wavelength than 3 µm. Besides solar absorption, thermal radiation of the object also should be considered. Not all the radiation is propagated to space, due to atmospheric affects. Only 87% of the radiation can be transferred to deep space in 8 µm – 13 µm wavelength range. Transmission of atmosphere can be seen figure below (Taylor, 1957).

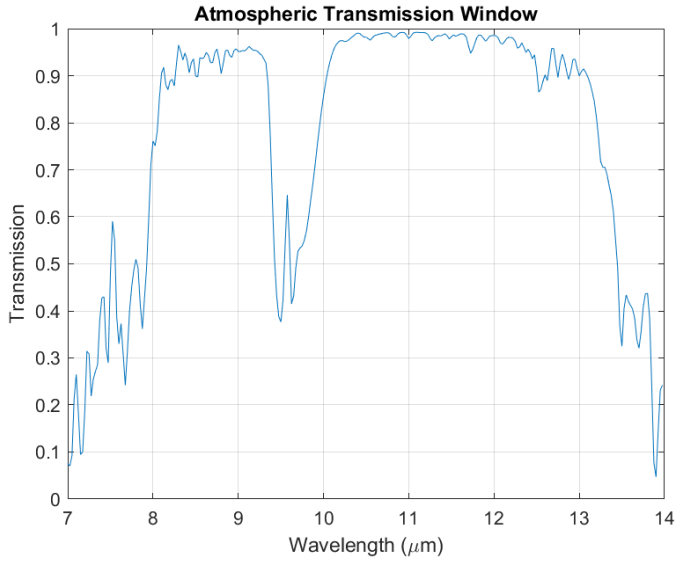

Figure 2-8 Atmospheric Transmissivity in 8 µm - 13 µm Band (Şuyun, 2023)

Table 4 Thermal Radiation Parameters

Parameter	Value
$\varepsilon_{0.3\ \mu m-3\ \mu m}$	0.75
$\varepsilon_{8\ \mu m-13\ \mu m}$	0.95
T_{sun}	5800K
k_B	$5.67*10^{-8}$ $Wm^{-2}K^{-4}$
h	6.63 J*s
$\lambda_{cut-off}$	3 µm
δ	$5.67*10^{-8}$
T_{object}	303K
T_{sky}	213K (Abbood, 2018)

Due to emissivity properties of fiberglass case, $P_{total}(T_{object})$ =435 W/m2 heat flux is calculated with the parameters mentioned in Table 4 are used in the equations 15 to 20.

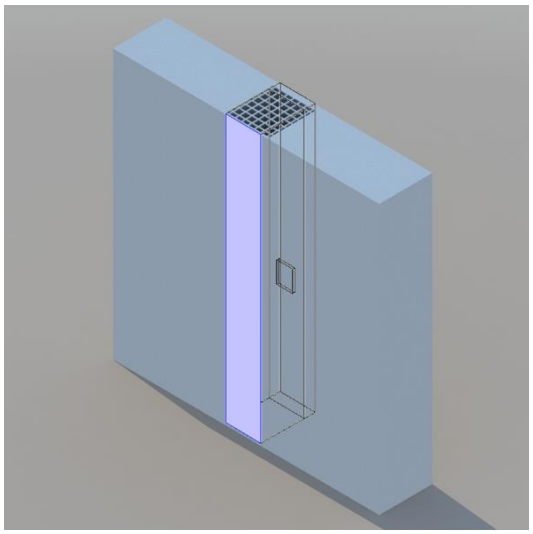

Figure 2-9 Surface Exposed to Thermal Radiation is Highlighted (Şuyun, 2023)

Only, front face of the box is subjected to solar irradiation due to orientation. Other walls of the shaft is assumed to be thermally insulated. The base plate electronic component attached to is assumed as FR4 which has a low thermal conductivity material widely used for printed circuit boards (Sarvar, 1990). Thus, it can be assumed as a thermally insulated surface. The

volume average of electronic component exceeds 55 degrees Celsius of operational temperature even at 5 Watts of power consumption as it can be seen in the Table 5. Effects of solar irradiation should be canceled out for better cooling performance.

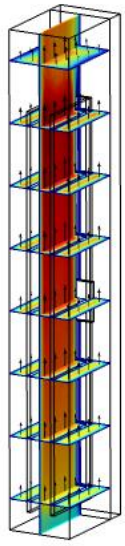

Figure 2-10 Natural Convection Flow Regime in the Shaft (Şuyun, 2023)

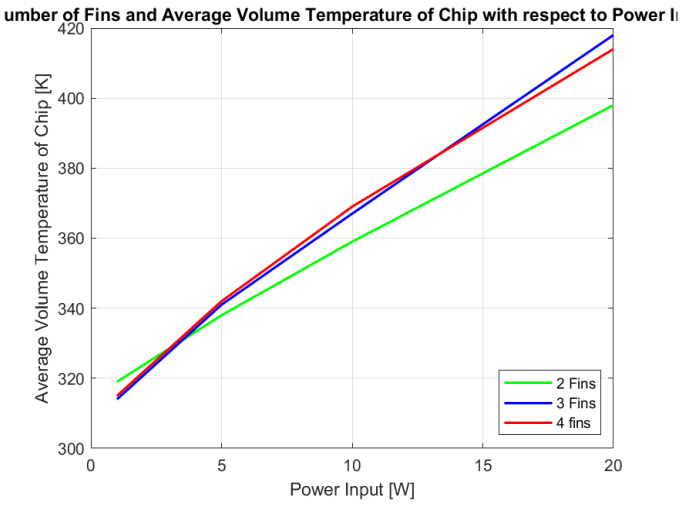

Figure 2-11 Number of Fins and Average Volume Temperature of Chip with respect to Power Input (Şuyun, 2023)

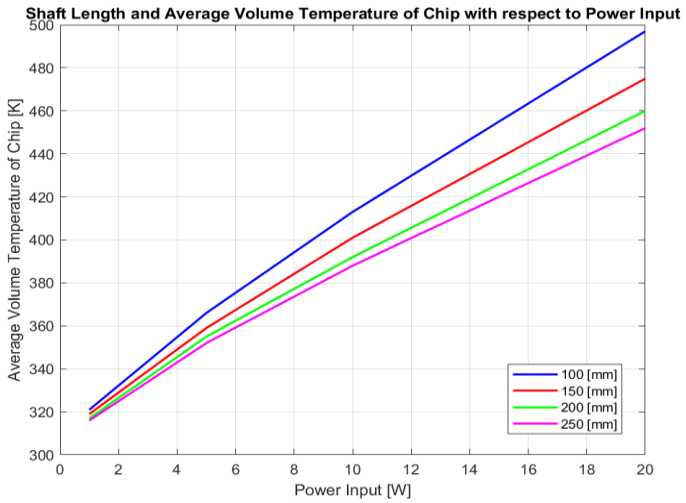

Figure 2-12 Fin Length and Average Volume Temperature of Chip with respect to Power Input (Şuyun, 2023)

Different numbers of fins are analyzed to achieve maximum heat dissipation. Width of the electronic component is 15 millimeters, as starting point 4 millimeters of fin spacing is selected. Which resulted in three fins. Increasing the number of fins resulted in lower heat dissipation, since viscous forces become more effective and stagnated the flow. Wider spacing between fins resulted in better performance for cooling.

Table 5 Heat Generated by Chip and Average Volume Temperature of Chip

Heat Generated by Chip	**Average Chip Temperature**
1 W	319K
5 W	338K
10 W	359K
20 W	398K

3. SPECTRALLY SELECTIVE MULTILAYER THIN FILMS FOR PRC APPLICATIONS

3.1. Problem Definition

In the previous chapter the effect of solar radiation shortens the lifetime of the chip to be used by increasing temperature of chip above 308K. One way to prevent this is to design a passive radiative cooling surface to be applied on base station box to decrease the heating due to solar radiation.

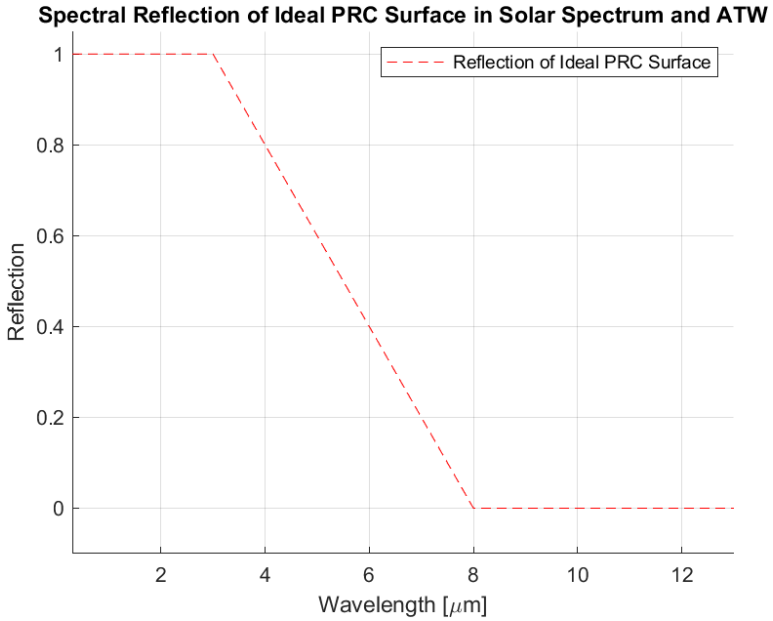

Figure 3-1 Reflection Characteristics of an Ideal PRC Surface (Şuyun, 2023)

Passive Radiative Cooling Systems require to reflect radiation within 0.3 μm – 3 μm wavelength range, meanwhile absorbing radiation within 8 μm – 13 μm range. Previous work

on heat reflective surfaces relied on multiple stacks of dielectric thin-films or patterns with multiple stacks (Raman AP, 2014; Wu JY, 2017; Suichi T, 2017; Kecebas MA, 2017; Chen, 2016). Multiple constructive interferences are used to increase reflectivity for desired applications. For PRC applications it is important to reflect radiation between wavelength range 300 nm – 3000 nm as shown in Figure 3-1. Stack of multilayer dielectric thin-films with specific thicknesses can achieve this reflection behavior. To be able to create a filter for such an application, complex optimization algorithms will be needed since reflection equation is non-linear. After creating governing equation, optimization algorithms will be used to optimize layer thicknesses.

3.2. Methodology

What percentage of the incoming radiation is reflected can be found with Fresnel's Laws (Orfanidis, 2016). When E-fields are perpendicular to the plane of incidence, it is denoted as s-polarized wave, and it is denoted as P-polarized when electric field is parallel to the plane of incidence. In Figure 3-2, components of incoming, reflected, and refracted beams are shown for S-Polarized Wave. Tangential component of the magnetic and electric field should be equal due to boundary conditions of dissimilar dielectric materials with refractive index n_i and n_t. Boundary conditions can be written as (Orfanidis, 2016):

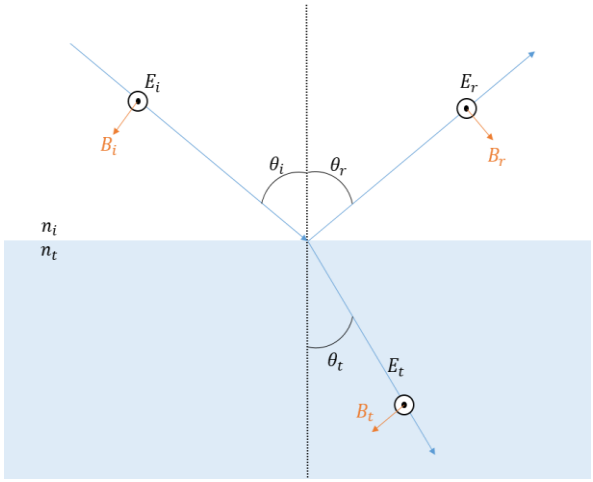

Figure 3-2 Electric and Magnetic Field in an Optical Interface (Şuyun, 2023)

Equation 21

$$E_i + E_r = E_t$$

Equation 22

$$B_i \cos\theta_i - B_r \cos\theta_r = B_t \cos\theta_t$$

Where,

θ_i:Angle of incident wave

θ_t:Angle of refraction

n_i:refractive index of incident media

n_t:refractive index of refracting media

E_i:Amplitude of electric field of incident wave

E_t:Amplitude of electric field of refracted wave

B_i:Amplitude of magnetic field of incident wave

B_t:Amplitude of electric field of refracted wave

Magnetic field can be written in terms of electric field with equation 23 where $c_0$the speed of the light is.

Equation 23

$$B = \frac{E * n}{c_0}$$

After writing magnetic field in terms of electric field, equation 21 is incorporated with equation 23. Reflection coefficient in s-polarization r_s which is defined as E_r/E_i yields to: Equation 24

$$\frac{E_r}{E_i} = r_s = \frac{n_i \cos\theta_i - n_t \cos\theta_t}{n_i \cos\theta_i + n_t \cos\theta_t}$$

For oblique incident (θ_i=θ_t=0) s-polarization and p-polarization reduces to same equation and r_s becomes:

$$\frac{E_r}{E_i} = r_s = \left|\frac{n_i - n_t}{n_i + t}\right|$$

And total reflected power R_s is:

$$R_s = r_s^2 \qquad (2.1.\text{-}5)$$

Since, material properties show difference with respect to radiation wavelength, aluminum slab show reflective behavior when exposed to radiation between 8 μm – 13 μm.
Single layer of aluminum spectral reflectivity is shown in Figure 3-3.

Figure 3-3 Aluminum Spectral Reflectivity *(Rakic, 2018)*

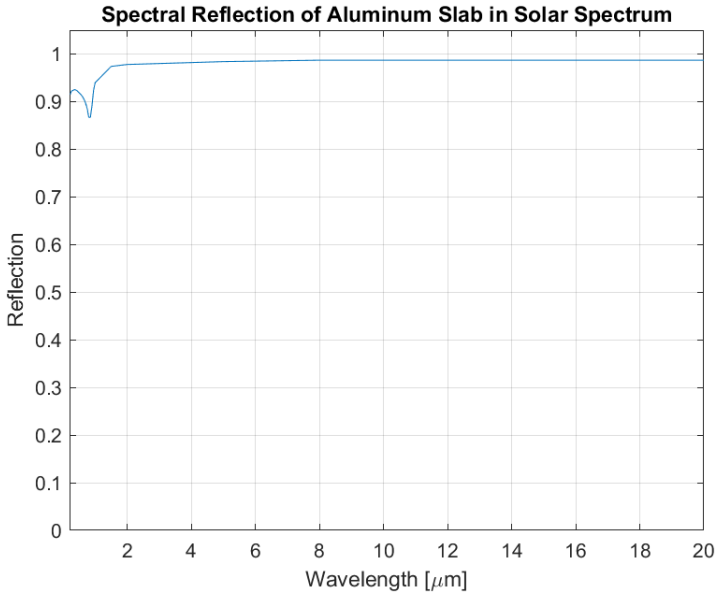

As it can be seen in Figure 3-3 aluminum reflects radiation in 0.2 μm – 20 μm range. To be able to absorb radiation in the mentioned range surface should be altered since aluminum is reflective material in the mentioned range. One way to decrease reflection of aluminum is

coat its surface with absorptive material. Optical properties of silicon nitride and silicon dioxide in the mentioned range can be seen in Figures 3-4 and 3-5 respectively. Both materials are lossless in shorter wavelengths, meanwhile they have a higher imaginary part of refractive index in atmospheric transmission window (green area). To improve absorption of aluminum surface in ATW one layer of silicon dioxide and one layer of silicon nitride is stacked over aluminum surface. Notice in Figure 3-4 and 3-5, both materials have lossy characteristics. To be specific silicon nitride has peak extinction coefficient in 11 μm of radiation, meanwhile this peak is smaller for silicon dioxide. For absorption characteristic to span through atmospheric transmission window both materials can be used together.

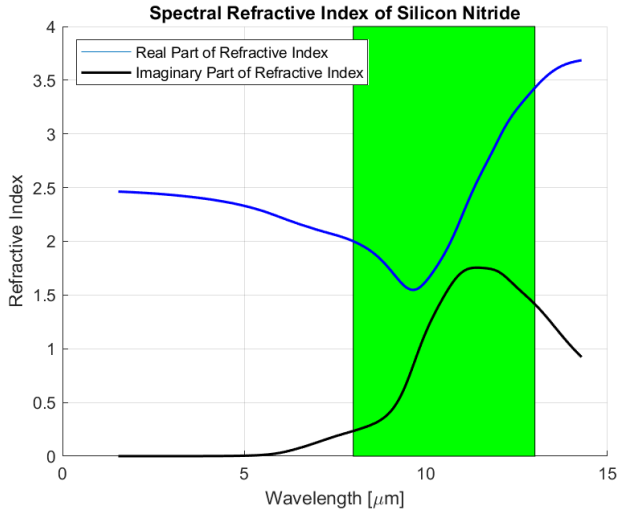

Figure 3-4 Spectral Refractive Index of Silicon Nitride Data Taken From *(Kischkat, 2012)*

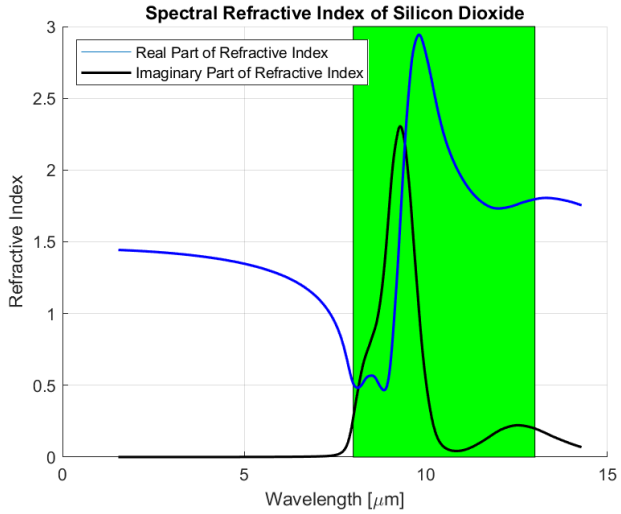

Figure 3-5 Spectral Refractive Index of Silicon Dioxide Data Taken From *(Kischkat, 2012)*

One way to disrupt reflection is creating destructive interference. Destructive interference can be obtained when reflected radiation and incoming radiation is in opposite phases. Also, if there happens to be a material which is absorptive in atmospheric transmission window and arranging thickness of such material would create absorptive behavior. Reflection measurements of surfaces are done with photonic simulation software Ansys Lumerical. Silicon dioxide and silicon nitride layers both have 3 µm thickness over aluminum slab. Three layers of materials with silicon nitride at top and silicon dioxide in the middle would create the following reflection in the mentioned range. After introducing Silicon Dioxide and Silicon Nitride to the aluminum base layer, reflection behavior can be seen in Figure 3-6.

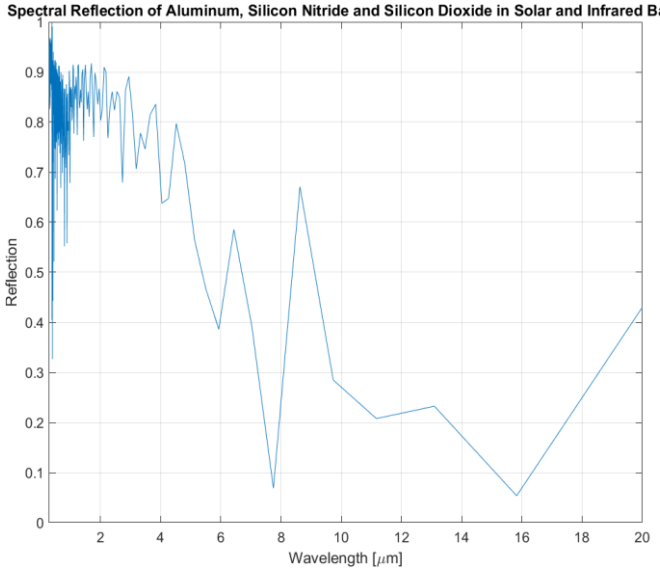

Figure 3-6 Reflection of Aluminum Slab Coated with Silicon Nitride and Silicon Dioxide (Şuyun, 2023)

Reflection characteristics decrease as the introduction of absorptive layer as it can be seen in Figure 3-6. So, extra measures needed to be taken to prevent performance drop of the surface.

To improve reflection performance of system in shorter wavelength novel design method is suggested in this chapter. A multilayer thin film system where high refractive index material and low refractive index material can offer adequate reflection characteristic. Selection of materials for reflective coating depends again on the refractive index of material in solar band. Silicon Nitride and Silicon Dioxide seems suitable combination in first glance, however titanium dioxide offers higher refractive index difference when used with silicon dioxide which results in better performance in means of reflection at shorter wavelengths.

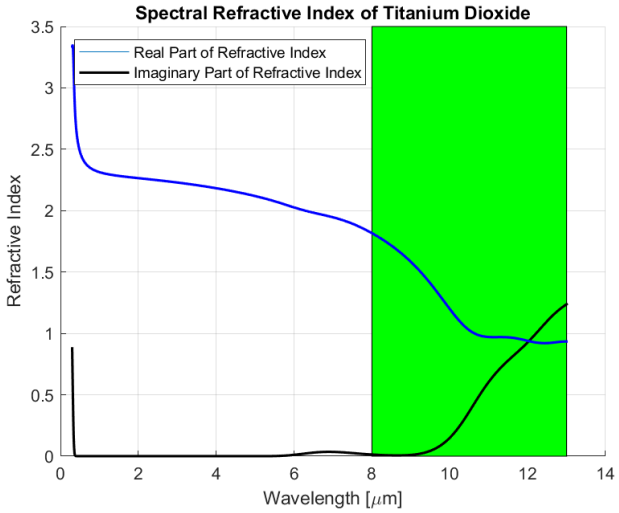

Figure 3-7 Spectral Refractive Index of Titanium Dioxide Data Taken From *(Kischkat, 2012)*

Uniform plane waves interfering with the dielectric multilayer films are expressed via following manner. It is assumed that direction of propagation is perpendicular to material interface. Since there are several interfaces, waves will be propagating forwards and backwards. Equation for a plane wave propagating in z-direction with x-polarization with respect to position z can be calculated via following method (Orfanidis, 2016):

Equation 25

$$E(z) = E_{0+}e^{-jkz} + E_{0-}e^{jkz} = E_{+}(z) + E_{-}(z)$$

Equation 26

$$H(z) = \frac{1}{\eta}\left[E_{0+}e^{-jkz} + E_{0-}e^{jkz}\right] = \frac{1}{\eta}\left[E_{+}(z) + E_{-}(z)\right]$$

Wave impedance Z(z) is expressed as:

Equation 27

$$Z(z) = \frac{E(z)}{H(z)}$$

Diffusing equation 26 and 27 together:

Equation 28

$$Z = \frac{E}{H} = \frac{[E_+(z) + E_-(z)]}{\frac{1}{\eta}[E_+(z) + E_-(z)]} = \eta \frac{1 + \frac{E_-}{E_+}}{1 - \frac{E_-}{E_+}} = \eta \frac{1 + \Gamma}{1 - \Gamma}$$

Where, η is characteristic impedance of the medium and equals to

Equation 29

$$\eta = \sqrt{\frac{\mu}{\varepsilon}}$$

optical thickness δ_i will be useful while calculating wave impedance of i-th layer.

Equation 30

$$\delta_i = \frac{2\pi n_i d_i}{\lambda}$$

Where,

n_i: $refractive\ index\ of\ the\ medium$

d_i: $thickness\ of\ the\ medium$

For multilayer system wave impedance can be found as

Equation 31

$$Z_i = \eta_i \frac{Z_{i+1} + j\eta_i \tan \delta_i}{\eta_i + jZ_{i+1} \tan \delta_i}$$

Figure 3-8 show electromagnetic waves travelling through multi-layer dielectric slabs.

Where,

η_i:Characteristic impedance of the $i^{th}\ layer$

η_i: $Free\ space\ impedance$

d_i: $Thickness\ of\ the\ i^{th}\ layer$

E_{i-}: $Forward\ propagating\ electromagnetic\ wave\ in\ the\ i^{th}\ layer$

E_{i+}: $Backward\ propagating\ electromagnetic\ wave\ in\ the\ i^{th}\ layer$

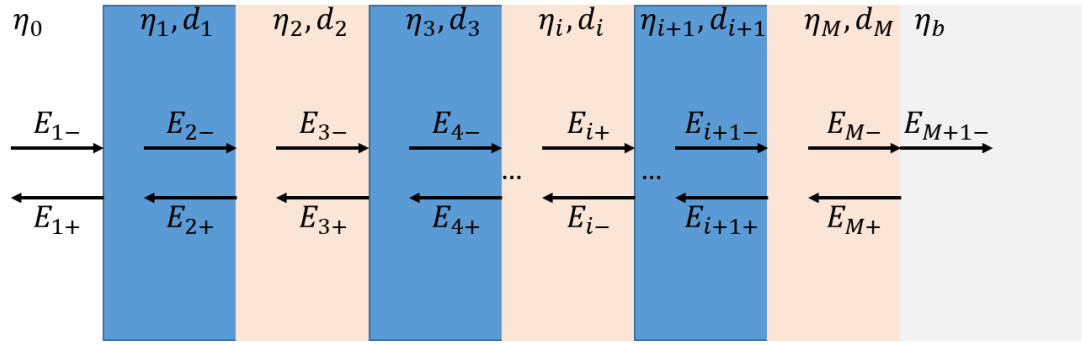

Figure 3-8 Multilayer Dielectric Structure (Şuyun, 2023)

For multilayer dielectric structure like above, governing equation of reflection reduces to Equation 32 *(Orfanidis, 2016)*

$$\Gamma = \frac{Z_1/Z_0 - 1}{Z_1/Z_0 + 1} = \frac{E_{1-}}{E_{1+}}$$

Equation 32 will be the governing equation for objective function for an optimization algorithm. Thicknesses of each layer will be variables to be tuned maximize reflection between 0.3 μm and 3 μm. Particle swarm optimization is used to optimize governing equations. Details of the algorithm will be explained in detail. 2 layers of material, with following sequence silicon oxide, titanium dioxide is selected to optimize. Titanium oxide is selected because it tends to reflect shorter wavelengths while it is highly transitive ATW range.

Layer order = [Titanium Dioxide; Silicon Dioxide]

Layer thicknesses = [x(1) x(2)]

Wavelength range to be is chosen as 0.3 μm – 0.9 μm range because aluminum sub-layer already reflects radiation with wavelength longer than 0.9 μm. This measure is taken to minimize computational effort. Geometry is defined with varying layer thicknesses as figure above. Optimization algorithm will randomly alter thicknesses of each layer while improving objective function in each iteration.

In each iteration algorithm that calculates reflection according to random thickness inputs [x(1) x(2)] in the desired wavelength range.

Then algorithm integrates reflection curve from 0.3 μm to 0.9 μm let's call it $\int_{0.3}^{0.9} R$

Equation 33

$$f_{objective} = -\int_{0.3}^{0.9} R$$

Algorithm tries to decrease $f_{objective}$ value, which results in increase of term ($\int_{0.3}^{0.9} R$) with 2-layer design. Particle Swarm Optimization (Kennedy, 1995) is used for the design.

Particle Swarm Optimization is a stochastic optimization algorithm that is used for non-linear, multi-parameter problems. The algorithm is created to mimic the behavior of swarm. All members of the swarm help to scan the solution space for the best combination. In this case, thickness of two layers are parameters to be altered. P number of particles are created for each parameter. In the t^{th} iteration, particle i's position is denoted as $X^i(t)$ which is defined by $X^i(t) = (x^i(t), y^i(t))$

Other than position imaginary velocity vector is also assigned to each particle. Each particle will start with a position on the solution domain and a velocity vector to span the solution domain. Velocity vector is defined by $V^i(t) = (v^i_x(t), v^i_y(t))$. For the next iteration new position of the particle is determined by;

Equation 34

$$X^i(t+1) = X^i(t) + V^i(t+1)$$

New x and y position of the particle is:

Equation 35

$$x^i(t+1) = x^i(t) + v^i_x(t+1)$$

Equation 36

$$y^i(t+1) = y^i(t) + v^i_y(t+1)$$

Meanwhile algorithm updates velocity of the particles with following manner;

Equation 37

$$V^i(t+1) = wV^i(t) + c_1 r_1 \left(p^i_{best} - X^i(t)\right) + c_2 r_2 \left(g_{best} - X^i(t)\right)$$

Where,

p^i_{best}:particle position that gives the best $f_{objective}$ by particle i

g_{best}:particle position that gives the best $f_{objective}$ by any particle

r_1:random number between 0-1

r_2:random number between 0-1

w:inertia weight constant, used to determine particles tendency to hold on its previous velocity

c_1:cognitive coefficient, used as weight of particles own results

c_2:social coefficient, used as weight of swarm's results

$p_{best}^i - X^i(t)$ is vector subtraction. When it is added to the $V^i(t)$, particles position becomes p_{best}^i, as the difference $g_{best} - X^i(t)$.

The social and cognitive coefficients are used to alter weight of particle's own experience or swarm's experience on iterations. The terms p_{best}^i and g_{best} are updated in each operation to notify best solution for objective function in each iteration.

Using this algorithm, the following parameters and reflection characteristics with these parameters are obtained for reflective layer.

Layer thicknesses = [113.5 nm 65 nm]

Layer order = [Titanium Dioxide; Silicon Dioxide]

Silicon Nitride top coating is applied to the top surface to obtain absorption in ATW band. Titanium dioxide layer is also added to top of the aluminum for better emissivity in ATW band. Final geometry is shown in Figure 3-9.

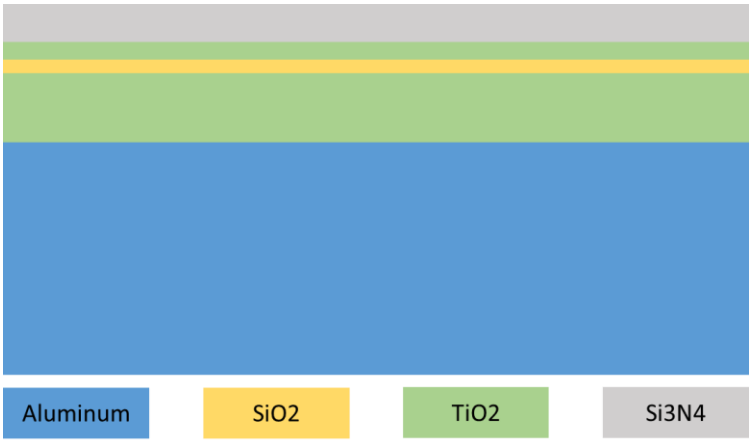

Figure 3-9 Final Geometry of Al-SiO2-TiO2-Si3N4 Multi-layer Thin Films (Şuyun, 2023)

Thickness of the layer from top to the bottom are:

[10 µm, 113.5 nm, 65 nm, 10 µm, semi-infinite]

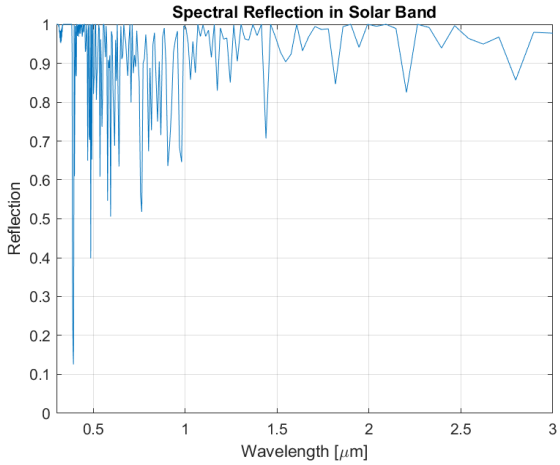

Figure 3-10 Spectral Reflection of Al-SiO2-TiO2-Si3N4 Multi-layer Thin Films in Solar Band (Şuyun, 2023)

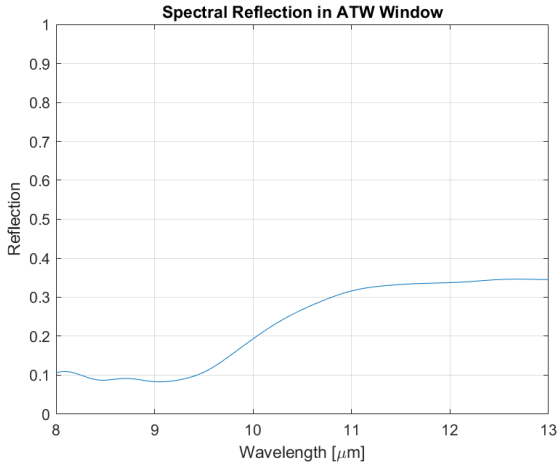

Figure 3-11 Spectral Reflection of Al-SiO2-TiO2-Si3N4 Multi-layer Thin Films in ATW (Şuyun, 2023)

As the introduction of reflective layers above the absorptive layers, reflection in solar band increased to 91%, and absorption in ATW increased to 80% with the final design.

4. SPECTRALLY SELECTIVE TITANIUM DIOXIDE EMBEDDED ACRYLIC FOR PRC APPLICATIONS

4.1. Problem Definition

At least one of the surfaces of the base station should transmit radio waves in super-high band. PRC surface designed and analyzed in the previous chapter includes aluminum surface as a bottom layer. Metals totally reflect radio waves so a new design without aluminum as sub-layer is required. A surface with metal sub-layer cannot be used since it would entrap electromagnetic waves in box. A new design with dielectric materials is required. To be able to obtain the same reflection as aluminum, more dielectric layers with specific thicknesses are needed. As layer numbers increase manufacturing costs also increase. A cheaper method is designed and tested.

4.2. Methodology

This solution makes use of scattering effect. Previous work on porous polymers relied on exotic plastics called P(VdF-HFP)HP and air pockets. In this thesis similar results are obtained with PMMA with titanium dioxide nanoparticles which is a more available

alternative to P(VdF-HFP)HP since titanium dioxide and PMMA is widely accessible in market. Firstly, PMMA should be checked if it is transmissive to super-high frequency radio waves. In this thesis the operating frequency of base station is selected in the 24-40 GHz range. Transmissivity of material depends on real and imaginary part of relative permittivity on frequency of interest (Kazemipour, 2014). Acrylic can be assumed as a single dielectric slab as follows.

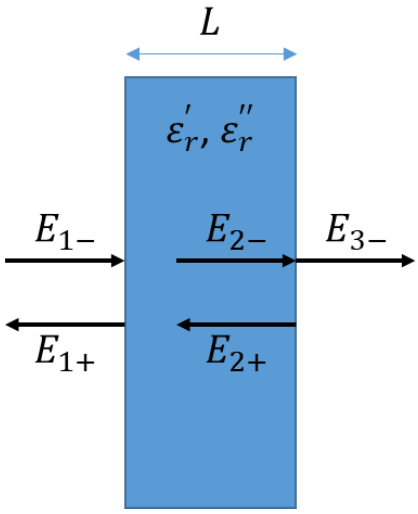

Figure 4-1 Single Dielectric Slab (Şuyun, 2023)

Blue area is considered as PMMA slab, where L is the width of the slab in Figure 4-1. For simplicity medium a and medium b are considered as air. Real and imaginary part of relative permittivity for PMMA at 24 to 40 GHz frequency(f) is (Palessonga, 2017):

$$\varepsilon_r' = 2.6$$

$$\varepsilon_r'' = 0.05$$

Where speed of electromagnetic waves in vacuum,

$$c_0 = 3 * 10^8 \, {}^{m}/_{s}$$

Transmission percentage of electromagnetic waves in a defined geometry is expressed as (Kazemipour, 2014):

$$|T| = \frac{E_{3-}}{E_{1-}} = \exp\left(-\frac{\varepsilon_r''}{\sqrt{\varepsilon_r'}} * \frac{\pi f L}{c_0}\right)$$

Where L is the thickness of the slab.

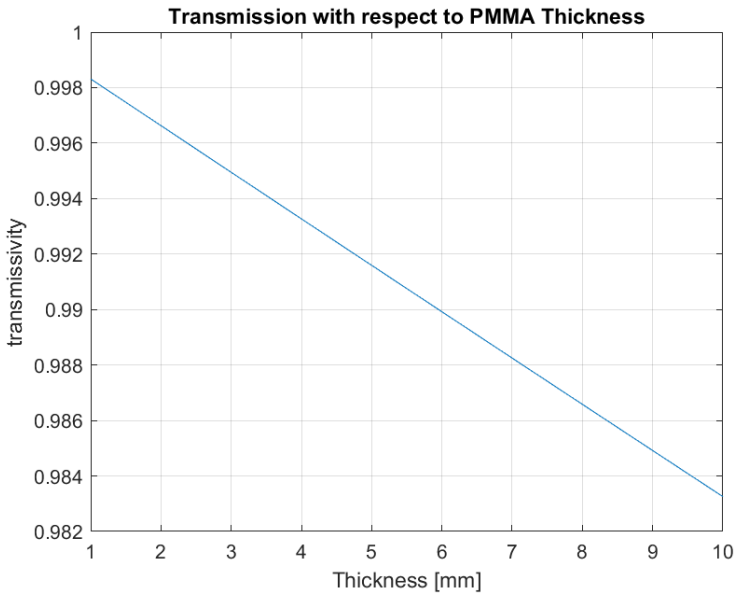

Figure 4-2 Spectral Transmission at 24 - 40 GHz Range with respect to PMMA Thickness (Şuyun, 2023)

Transmission of electromagnetic waves through PMMA (Acrylic) slab remain high although its thickness is increased to 10 mm. Reduce in power while electromagnetic waves propagate through the PMMA slab is negligible since it is smaller than 0.6% for 3 mm slab. Thus, it can be used for the surface which propagation will take place.

The same procedure will be done also for titanium dioxide since acrylic itself is not reflective in solar spectrum. Titanium Dioxide is suitable for solar reflective coating since it is lossless and has high refractive index in shorter wavelengths. Relative dielectric properties of titanium dioxide are (Freitas, 2020):

$$\varepsilon_r' = 58$$

$$\varepsilon_r'' = 0.05$$

Figure 4-3 TiO2 Transmissivity at GHz Frequencies (Şuyun, 2023)

Total thickness of titanium dioxide will be fewer than 1 millimeter. At least 98% of the propagation can pass through the titanium dioxide layer. Thus, titanium dioxide can be used in the propagation surface.

Titanium dioxide is widely available in the market in powder form. As the grains of Titanium dioxide get smaller more scattering affect can be obtained in smaller distances. However, design should be tolerant to particle sizes since Titanium dioxide powders that you can find in the market have all kind of particle sizes inside. Titanium dioxide should be lossless in solar band to be used in reflective coating. Titanium dioxide nanospheres with 0.1 μm – 0.3 μm and 0.5 μm radius are tested under radiation in the 0.3 μm – 3 μm wavelength range if they are lossless. Commercially available FDTD program Ansys Lumerical is used to determine absorption characteristics of nanoparticles. Absorption characteristics of titanium dioxide nanoparticles are shown in Figure. Notice, absorption is low in solar band and only increases to 10% around 350 nm wavelength. Average absorption of titanium dioxide nanoparticles is around 1%, thus absorption can be neglected during calculations.

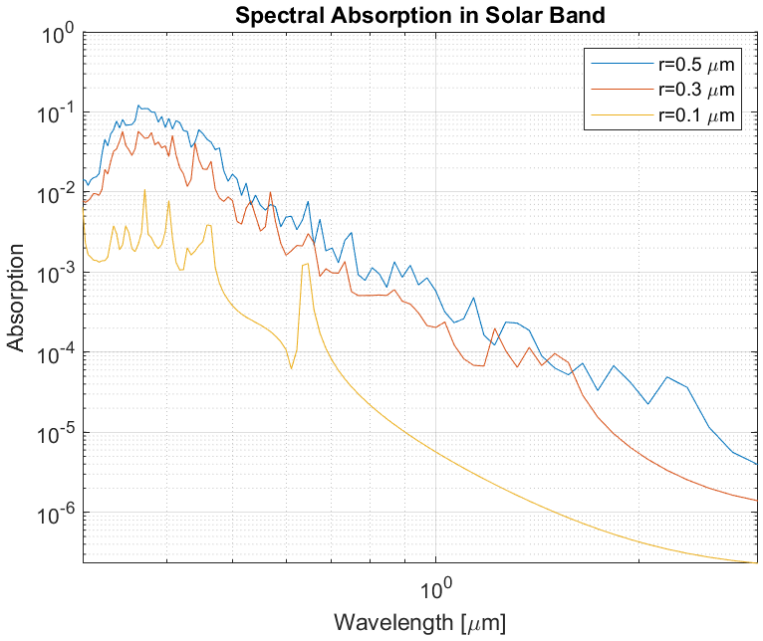

Figure 4-4 Absorption of TiO2 Nanoparticles with respect to Radius (Şuyun, 2023)

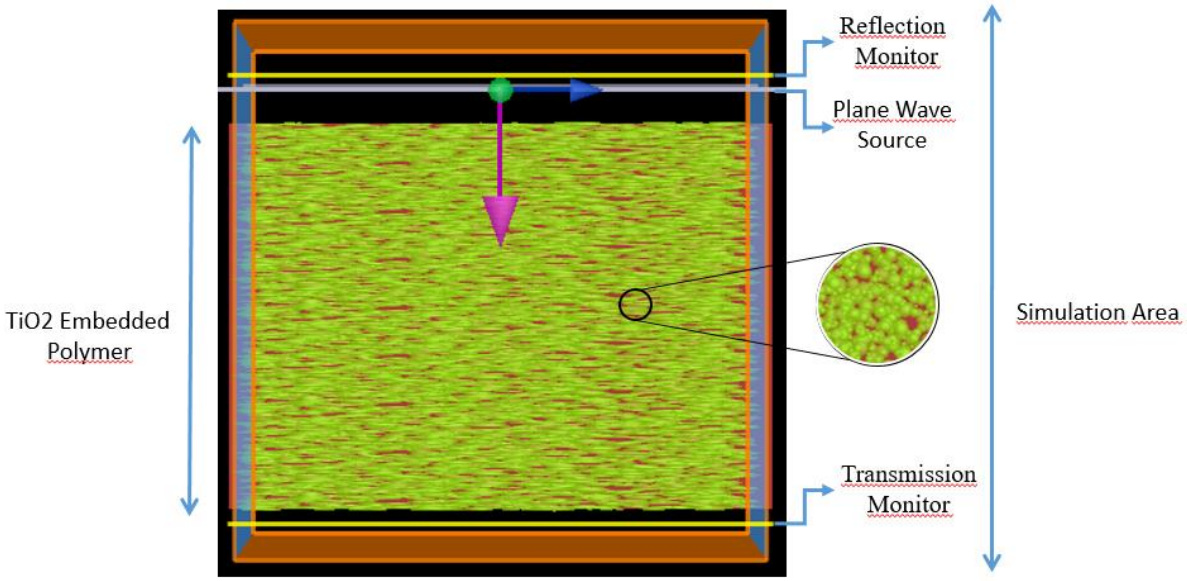

Figure 4-5 FDTD Simulation Setup (Şuyun, 2023)

FDTD simulator setup shown in Figure 4-5 is obtained by the parameters in Table 6.

Table 6 FDTD Simulation Parameters

Description	Value
Particle Sizes	0.1 µm, 0.3 µm, 0.5 µm
Particle Distribution	Linearly Random
Volume Ratio of TiO2 to PMMA	16%
Total Thickness	80 µm

Results for reflection are calculated using the R=1-T-A formulation (Dyachenko, 2014).

Where A and T are absorption and transmission respectively. Reflection response obtained from titanium dioxide embedded PMMA can be seen in Figure 4-6. To decide thickness of the coating, sensitivity analysis is done. Increasing the thickness of the coating did not improve results. Thus, maximum thickness of 80 µm is simulated.

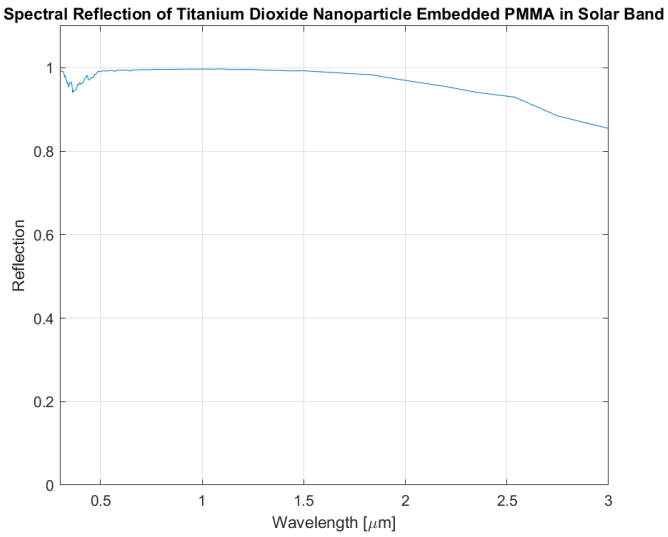

Figure 4-6 Spectral Reflection of TiO2 Embedded PMMA in Solar Band (Şuyun, 2023)

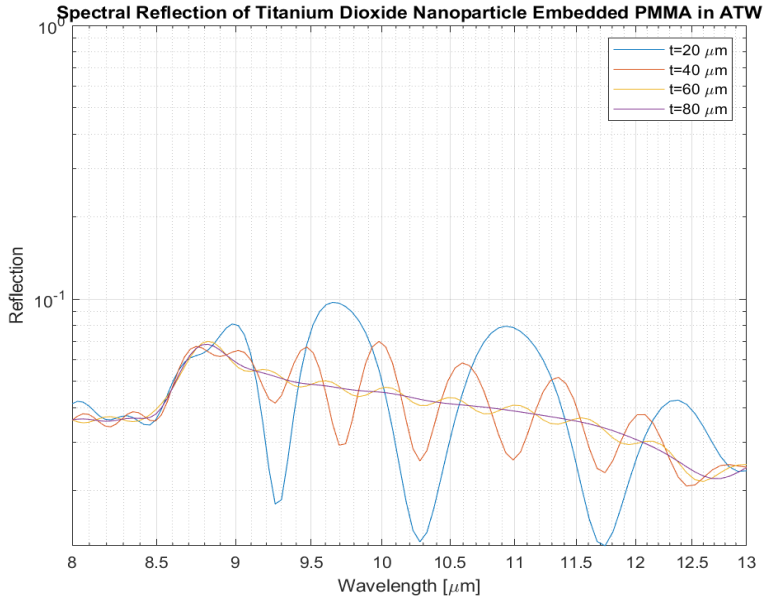

Figure 4-7 Spectral Reflection of TiO2 Embedded PMMA in ATW (Şuyun, 2023)

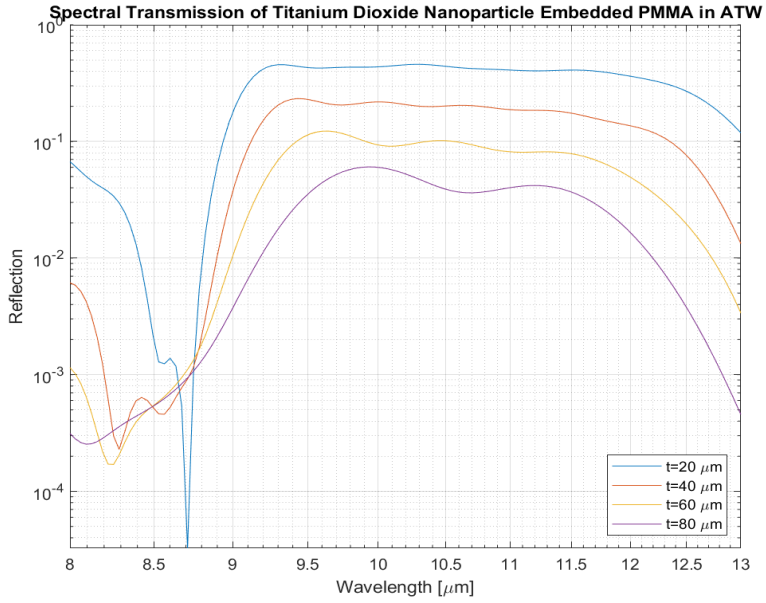

Figure 4-8 Spectral Transmission of TiO2 Embedded PMMA in ATW (Şuyun, 2023)

As thickness increases in the design absorption does not change drastically in average. However, transmission decreases with the increase in thickness, which is a desired result to avoid any reflection from the surface beneath design.

An average of 98% reflection is obtained in solar band, meanwhile average reflectivity in ATW is 4%.

5. SIMULATION, ANALYSIS & RESULTS

Cooling of base stations requires electricity as much as their electric demand for communication operations. To be able to reduce carbon footprint of 5G communication, passive cooling systems can come to the aid. Passive radiative cooling (PRC) is a cooling method which does not require any energy input during operation. Excess energy is transferred to outer space with thermal radiation, while sunlight is reflected. For PRC surface, there are two requirements that should be fulfilled. The body should radiate thermal energy to outer space. Not all the radiated thermal energy can be transferred to outer space. Our atmosphere has a gap between that allows radiation between 8 μm and 13 μm wavelength to dissipate to outer space. Net cooling of a PRC surface can be calculated by considering radiated thermal energy, absorbed solar energy. The cooling power of the designed surfaces can be found with the same procedure as defined in Chapter II. Absorption characteristics can be related to emissivity with Kirchoff's Law of Thermal Radiation. An object which emits and absorbs thermal radiation, emissivity is equal to absorptivity. Thus, emissivity ϵ equals absorption α.

Emissivity of thin-films designed in Chapter II, in solar and infrared band are

$$\varepsilon_{0.3\ \mu m-3\ \mu m} = 0.09$$

$$\varepsilon_{8\ \mu m-13\ \mu m} = 0.81$$

Solar radiation, radiation from sky and ambient, heat generated within object, conduction and convection heat flux and radiated heat from object are the terms affecting the thermal

equations. The temperature of object is assumed to be the same as the ambient temperature to simplify equations. Heat generated by the object and heat transfer due to convection calculated by computational fluid dynamics commercial program. So, three terms are calculated for the thermal radiation equations and superposed in commercial program. Conduction heat transfer is also assumed as negligible since air surrounds the box and is only connected with small connection elements.

With the assumptions above heating power becomes (Howell, 2021);

$$P_{total}(T_{object}) = P_{rad}(T_{object}) - P_{sun}(T_{sun})$$

Where;

$$P_{rad}(T_{object}) = A \int d\Omega \cos\theta \int_0^{\infty} d\lambda I_{BB}\left(T_{object}, \lambda\right)\epsilon(\lambda, \theta)$$

Where,

A:Area of the object

The front face of the rectangular shaft in the middle of the 5G small cell 5 cm width and 25 cm height. Thus, the area is equal to 125 cm^2.

$\int d\Omega$:Angular integral over a sphere

$I_{BB}(T_{object},\lambda)$:Spectral radiance of a blackbody at temperature T_{object}

λ:Spectral angular emissivity

$$I_{BB}(T_{object}, \lambda) = \frac{2hc^2}{\lambda^5} \frac{1}{e^{hc/(\lambda k_B T_{object})} - 1}$$

Where;

h:Planck's constant

k_B:Boltzmann constant

c:Speed of light

λ:wavelength

Absorbed power due to incident atmospheric thermal radiation can be calculated as:

$$P_{sun} = A \int_0^{\infty} d\lambda \epsilon(\lambda, \theta_{sun}) I_{AM1.5}(\lambda)$$

Where,

$I_{AM1.5}(\lambda)$: $Spectral\ Solar\ Irradiance$ $(1000\ W/m^2)$ (ASTM International, 2022)

Flat plate with 125 cm^2 with a fixed angle with respect to sun is assumed, so angular dependency on absorbed solar power is neglected. As mentioned in Chapter II, 98% of the solar radiation happens in wavelengths smaller than 3 μm. Also, not all of the radiation is propagated to space, due to atmospheric affects 87% of the radiation can be transferred to deep space.

All the walls except the front face were thermally insulated. Adding passive radiative cooling surface created a cooling effect of 1W, and it can change due to location of the box and the small area of the front face. However, it is considered that it does not heat up even in the worst possible scenario. It is safe to assume that the front face is also thermally insulated in COMSOL simulation setup. With the thermal insulation assumed new analyses show that chip can safely operate in 5W of power.

Results are:

Table 7 Heat Generated by Chip and Average Chip Volume Temperature

Heat Generated by Chip	**Average Chip Temperature**
1 W	319K
5 W	338K
10 W	359K
20 W	398K

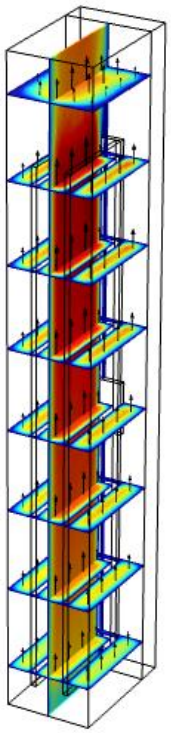

Figure 5-1 Natural Convection Flow Regime Calculated by COMSOL (Şuyun, 2023)

Table 8 Comparison of average chip temperature with and without PRC surface

Heat Generated by Chip	**Average Chip Temperature without PRC Surface**	**Average Chip Temperature PRC Surface**
1 W	319K	310K
5 W	338K	331K
10 W	359K	354K
20 W	398K	394K

For safe operation up to 20 W of heat dissipation by chip forced convection can be used. A fan with 5W of power consumption generating 16 CFM of volumetric flow rate can create cooling effect that is enough to cool chip to suitable operating temperature.

Table 9 Heat Generated by Chip and Average Volume Temperature under Forced Convection

Heat Generated by Chip	**Temperature under Forced Convection with Parallel Plate Heat Sink with 16 CFM**
1 W	301K
5 W	306K
10 W	311K
20 W	323K

6. DISCUSSION

Analysis and simulations related to this research suggests that natural convection is not enough to cool a small cell base station under solar radiation. With the help of radiative cooling, small cells operating with 5 W of power, can be cooled without any power consumption for cooling system. PRC surfaces are widely used for buildings in literature and this paper is one of the first researches that investigates applicability of PRC surfaces for communication systems. If an electronic component generated more heat in the same volume, active cooling solutions are required. If heat transfer within the small cell, can be more uniformly distributed better passive cooling performances can be obtained. Previous research on PRC surfaces also investigates flat plate under the solar radiation. Exact cooling capacity for a 5G small cell box can be measured with empirical methods since exact capacity of PRC surfaces can change with respect to humidity, weather condition, altitude, position of the box and the tilt angle of the box etc.

In means of manufacturability of thin films magnetron sputtering with additional microwave source is presented by researchers (Mazur, 2016). However, the process needs to be precisely controlled and is not suitable for mass production. Solar reflective nanoparticles with absorption characteristic in ATW, are more suitable for mass production.

7. CONCLUSION AND FUTURE WORK

The focus of this research was to investigate sustainable cooling methods which do not require any power input to operate. Based on the simulations done with COMSOL Multiphysics program, it can be concluded that electricity-free cooling is possible to some extent. However, PRC surfaces show its value in bigger volumes with lower heat generated per unit volume such as buildings. Buildings with large number of electronics can also be areas of interest for energy free passive radiative cooling.

Bibliography

A. Bar-Cohen, W. M. (1984). Thermally optimum spacing of vertical, natural convection cooled, parallel plates. *ASME Journal of Heat and Mass Transfer*, 116-123.

Abbood, Z. M.-T. (2018). CALCULATION OF ABSORPTION AND EMISSION OF THERMAL RADIATION BY CLOUDS COVER. *ARPN Journal of Engineering and Applied Sciences*, 9446-9456.

Adibekyan, A. K. (2019). Review of PTB measurements on emissivity, reflectivity and transmissivity of semitransparent fiber-reinforced plastic composites. *International Journal of Thermophysics*, 36.

ASIAC. (1989). *U.S. Air Force Avionics Integrity Program notes.*

ASTM International. (2022). *ASTM E490-22.*

Black, J. R. (1969). Electromigration—a brief survey and some recent results. *IEEE Transactions on Electron Devices*, 338–347.

Cary, R. H. (1974). *Avionic radome materials.* NTIS.

Chang, K.-C. C.-C.-C.-C. (2020). Energy Saving Technology of 5G base station based on internet of things collaborative control. *IEEE Access*, 32935 - 32946.

Chen, Z. Z. (2016). Radiative cooling to deep sub-freezing temperatures through a 24-h day–night cycle. *Nature communications*, 13729.

Chih-Lin I, S. H. (2020). Energy-efficient 5G for a greener future. *Nature Electronics*, 182-184.

creativecommons. (2023). *Small Cell situated in the terrace of a building. .* Bangalore, India. Retrieved from wikimedia.

Çengel, Y. A. (2007). *Heat and mass transfer: A practical approach.* Tata McGraw-Hill.

Dyachenko, P. N. (2014). Ceramic photonic glass for broadband omnidirectional reflection. *ACS Photonics*, 1127–1133.

Freitas, A. E. (2020). Development and Characterization of Titanium Dioxide Ceramic Substrates with High Dielectric Permittivities. *Materials*, 386.

Harrison AW, W. M. (1978). Radiative cooling of TiO2 white paint. *Solar Energy*, 185-188.

Howell, J. R. (2021). *Thermal radiation heat transfer.* CRC Press.

Huang Y, P. M. (2018). Broadband metamaterial as an “invisible” radiative cooling coat. *Optics Communications*, 204-207.

Incropera, F. P. (1969). Convection heat transfer in electronic equipment cooling. *Journal of Heat Transfer*, 1097–1111.

Jiang, L. H. (2023). Research on location planning of 5G base station based on DBSCAN clustering algorithm. *IEEE 2nd International Conference on Electrical Engineering, Big Data and Algorithms* (pp. 669-675). IEEE.

KAMINSKI, D. A. (2017). *Introduction to thermal and fluids engineering.* JOHN WILEY.

Kazemipour, A. H.-O. (2014). A reliable simple method to extract the intrinsic material properties in millimeter/sub-millimeter wave domain. *29th Conference on Precision Electromagnetic Measurements* (pp. 576-577). IEEE.

Kecebas MA, M. M. (2017). Passive radiative cooling design with broadband optical thin-film filters. *Journal of Quantitative Spectroscopy and Radiative Transfer*, 179-186.

Kennedy, J. &. (1995). Particle swarm optimization. *Proceedings of ICNN'95-international conference on neural networks* (pp. 1942-1948). IEEE.

Kischkat, J. P. (2012). Mid-infrared optical properties of thin films of aluminum oxide, titanium dioxide, silicon dioxide, aluminum nitride, and silicon nitride. *Applied Optics*, 6789-6798.

Koucheh, A. B. (2021). Impedance mismatch-based enhancement of broadband reflectance of tungsten with bio-inspired multilayers. *Journal of Quantitative Spectroscopy and Radiative Transfer*, 276.

Lee, S. (1995). Optimum Design and Selection of Heat Sinks. *IEEE Transactions on Components, Packaging, and Manufacturing Technology*, 812-817.

Macleod, H. A. (2021). *Thin-film optical filters.* CRC Press.

Mandal, J. F. (2018). Hierarchically porous polymer coatings for highly efficient passive daytime radiative cooling. *Science*, 315-319.

Mazur, M. W. (2016). Functional photocatalytically active and scratch resistant antireflective coating based on TiO2 and SiO2. *Applied Surface Science*, 165-171.

Michell D, B. K. (1979). Radiation cooling of buildings at night. *Applied Energy*, 263-275.

Mingjie Feng, S. M. (2017). Base station on-off switching in 5G wireless networks: Approaches and challenges. *IEEE Wireless Communications*, 46-54.

Orfanidis, S. J. (2016). *Electromagnetic waves and antennas.* Sophocles J. Orfanidis.

Ozisik, M. N. (1985). *Heat Transfer: A Basic Approach.* McGraw.

Palessonga, D. E. (2017). Bandwidth improvement of microwave photonic components based on electro-optic polymers loaded with tio2 nanoparticles. *Applied Physics A*, 1-10.

Pedram, M. N. (2006). Thermal modeling, analysis, and management in VLSI circuits: Principles and methods. *Proceedings of the IEEE*, 1487-1501.

Piegari, A. F. (2018). *Optical thin films and coatings: From materials to applications.* Woodhead Publishing.

Rakic, A. D. (2018). Algorithm for the Determination of Intrinsic Optical Constants of Metal Films: Application to Aluminum. *Advances in Engineering Software*, 31-49.

Raman AP, A. M. (2014). Passive radiative cooling below ambient air temperature under direct sunlight. *Nature*, 540-544.

Rang Tu, X.-H. L. (2010). Energy performance analysis on telecommunication base station. *Energy and Buildings*, 315-325.

Remsburg, R. (2017). *Thermal Design of Electronic Equipment.* CRC Press.

Sarvar, F. P. (1990). PCB glass-fibre laminates: Thermal conductivity measurements and their effect on simulation. *Journal of electronic materials*, 1345-1350.

Schaller, R. R. (1997). Moore's law: past, present and future. *IEEE spectrum*, 52-59.

Scott, A. W. (1976). *Cooling of Electronic Equipment.* AUC.

Small Cell situated in the terrace of a building. (2023). Retrieved from Wikimedia: https://commons.wikimedia.org/wiki/File:Small_Cell_by_Samsung.jpg

Sohel Murshed, S. M. (2017). A critical review of traditional and emerging techniques and fluids for electronics cooling. *Renewable and Sustainable Energy Reviews*, 821–833.

Suichi T, I. A. (2017). Structure optimization of metallodielectric multilayer for high-efficiency daytime radiative cooling. *Thermal Radiation Management for Energy Applications*.

Taylor, J. H. (1957). Atmospheric transmission in the infrared. *Journal of the Optical Society of America*, 223-226.

Wikimedia. (2010). Retrieved from Pin fin, straight fin and flared heat sinks: https://commons.wikimedia.org/wiki/File:Pin_fin,_straight_fin_and_flared_heat_sinks.png?uselang=en#Licensing

Willey, R. R. (2019). *Practical design and production of optical thin films.* CRC Press.

Wu JY, G. Y. (2017). Diurnal cooling for continuous thermal sources under direct subtropical sunlight produced by quasi-Cantor structure. *Chinese Physics B*, Vol. 26, No. 10.

Wypych, A. B.-K. (2014). Dielectric properties and characterisation of titanium dioxide obtained by different chemistry methods. *Journal of Nanomaterials*, 1-9.

Zhang, X. (2017). Metamaterials for perpetual cooling at large scales. *Science*, 1023-1024.

Zhao, B. H. (2019). Radiative cooling: A review of fundamentals, materials, applications, and prospects. *Applied Energy*, 489–513.